

## ABSTRACT

CALDERON, VICTOR ALEJANDRO. Condition Dependent Performance Based Seismic Design.  
(Under the direction of Dr. Mervyn Kowalsky.)

Structures located in seismic regions are often subjected to multiple earthquakes. Multiple earthquakes can accumulate damage resulting in a deterioration of the seismic performance of a structure. In addition, aging of the structure can lead to corrosion that further propagates the deterioration. Past research has shown that the Park and Ang damage index (DI)(a demand parameter that quantifies damage) increases as damage aging conditions in the structures worsen or multiple seismic events are included in the analysis. This increases the probability of structures to collapse. This research proposes to study the effects of multiple earthquakes and damage accumulation in RC structures by developing strain based fragility functions for different aging conditions. To achieve this it is also important to develop limit states that represent corroded reinforcing steel. Therefore, a method to perform accelerated corrosion in passivated reinforcing steel rebars is proposed. These corroded rebars are then subjected to tension tests and buckled bar tension tests, which will be used to define service and damage control limit states. To show the relevance of this study a framework that incorporates corrosion models into a nonlinear time history analysis (NLTHA) is developed. A series of SDOF cantilever columns are subjected to a sweep of earthquakes. Preliminary results show that there is an increase in the probability of reaching a limit state when corrosion level increases. The results also show large dispersion of results when using PGA as the intensity measure (IM), indicating the need for a better intensity measure. The results of this research will (1) develop fragility curves that consider strain limit states to measure damage while incorporating different aging conditions, (2) establish limit states for corroded rebars, (3) inform the research community on the necessary methodology to accurately model corrosion for material testing and large scale testing of corroded reinforced members (4) consider the effects of multiple earthquakes with mainshock-aftershock sequences (5) incorporate the results into the direct displacement-based design methodology.

© Copyright 2022 by Victor Alejandro Calderon

All Rights Reserved

Condition Dependent Performance Based Seismic Design

by  
Victor Alejandro Calderon

A thesis submitted to the Graduate Faculty of  
North Carolina State University  
in partial fulfillment of the  
requirements for the Degree of  
Doctor of Philosophy

Civil, Construction, and Environmental Engineering

Raleigh, North Carolina

2022

APPROVED BY:

---

Dr. James Nau

---

Dr. Mohammad Pour-Ghaz

---

Dr. Rudolf Seracino

---

Dr. Thomas Birkland

---

Dr. Mervyn Kowalsky  
Chair of Advisory Committee

## **DEDICATION**

To God, "How much better it is to get wisdom than gold! And to get understanding is to be chosen above silver" (Prov 16:16).

To my parents Victor M. Calderon and Roxana P. de Calderon, for all their love and support through the years and through the miles.

To my wife Aubrey, "If it takes doing a Ph.D. for us to meet it would have been worth it".  
Thank you for your love, support, patience and for filling my days with joy.

## BIOGRAPHY

I was born in San Salvador, El Salvador. I attended the Universidad Centroamericana José Simeón Cañas, where I graduated as Civil Engineer in 2012. Subsequently, I started working for the structural engineering consulting firm JEP Ingenieros y Arquitectos, where I gained experience designing Commercial buildings, schools and residential buildings. While still being a part of JEP, I pursued my Master in Civil Engineering at NC State 2014-2016. In 2016, I started to work for a hydropower company, where I was part of the team that designed the facilities for a large dam project. In the Spring 2018, I decided to return to NC State for the PhD program. In 2021, I became a registered Professional Engineer in the State of North Carolina. Going forward, I plan to continue my career as a structural engineer in a consulting firm.

## **ACKNOWLEDGEMENTS**

I would like to thank Dr. Kowalsky for his help. The Staff and Students at The Constructed Facilities Lab (CFL) at NC State. Analytical Instrumentation Facility (AIF) at NC State. The Center for Additive Manufacturing and Logistics (CAMAL) at NC State. The Alaska Department of Transportation and Public Facilities (AKDOT P&F).

## TABLE OF CONTENTS

<b>LIST OF TABLES . . . . .</b>	<b>vii</b>
<b>LIST OF FIGURES . . . . .</b>	<b>viii</b>
<b>Chapter 1 Introduction . . . . .</b>	<b>1</b>
1.1 Scope and layout . . . . .	3
<b>Chapter 2 Literature review . . . . .</b>	<b>4</b>
2.1 Corrosion . . . . .	4
2.1.1 Time to corrosion . . . . .	5
2.1.2 Rate of corrosion . . . . .	6
2.1.3 Corrosion modified properties of reinforcing steel bars . . . . .	8
2.1.4 Physical test on corroded RC Structures . . . . .	9
2.2 Steel strain aging . . . . .	11
2.2.1 Metallurgical process . . . . .	11
2.2.2 Strain aging effects in structures . . . . .	12
2.3 Damage Indexes . . . . .	13
2.4 Multiple earthquake loading . . . . .	16
2.4.1 Mainshock-aftershock sequences loading . . . . .	16
2.4.2 Mainshock sequences loading . . . . .	19
2.5 Aging of structures . . . . .	20
2.6 Research Gap . . . . .	22
2.6.1 Objectives . . . . .	23
<b>Chapter 3 Experimental program: mechanical properties and performance of corroded rebars . . . . .</b>	<b>24</b>
3.1 Proposed experimental campaign . . . . .	24
3.2 Expected outcomes from experimental phase . . . . .	36
<b>Chapter 4 Experimental Results from Corroded Rebar Specimens . . . . .</b>	<b>37</b>
4.1 Measurement of corrosion level . . . . .	37
4.2 Tensions Tests . . . . .	37
4.2.1 Yield strength as a function of corrosion . . . . .	39
4.2.2 Effect of corrosion in uniform elongation . . . . .	40
4.3 Buckled Bar Tension (BBT) Tests . . . . .	41
4.3.1 Summary of BBT procedure . . . . .	41
4.3.2 Effect of corrosion in Critical Bending Strain . . . . .	41
4.3.3 Effect of corrosion at the micro-structural level . . . . .	45
4.3.4 Effect of geometry imperfections . . . . .	48
<b>Chapter 5 Analytical model . . . . .</b>	<b>50</b>
5.1 Modeling of aging conditions . . . . .	50
5.1.1 Modeling of corrosion for structural analysis . . . . .	50

5.1.2	Modeling of strain aging for structural analysis . . . . .	51
5.2	Multiple seismic events . . . . .	51
5.2.1	Earthquake selection . . . . .	52
5.2.2	Modeling of mainshock-aftershock series for corrosion damage state . . . . .	54
5.2.3	Modeling of mainshock-aftershock series for strain aging damage state . . . . .	54
5.3	Analytical Model . . . . .	57
5.3.1	Cantilever column . . . . .	57
5.3.2	Strain penetration . . . . .	59
5.3.3	Design limit states . . . . .	60
5.4	Comparison with existing physical tests . . . . .	61
5.4.1	Pristine condition columns . . . . .	61
5.4.2	Accelerated corrosion columns . . . . .	62
5.5	Analytical framework . . . . .	64
5.6	Results from NLTHA . . . . .	65
5.6.1	Effect on structure response . . . . .	65
5.6.2	Development of cumulative distribution functions . . . . .	66
5.6.3	Results discussion . . . . .	68
5.7	Future topics . . . . .	68
<b>Chapter 6 Condition dependent performance based design and Assessment</b>	69	
6.1	Recommendations to new designs from material tests . . . . .	70
6.2	Design of new structures with consideration of aging conditions . . . . .	70
6.2.1	Existing methodologies . . . . .	70
6.2.2	Proposed methodology . . . . .	70
6.2.3	Application example: Bridge 547 (AKDOT) . . . . .	70
6.3	Assessment of existing structures considering aging conditions . . . . .	70
6.3.1	Existing methodologies . . . . .	70
6.3.2	Proposed Condition Dependent Performance Based Seismic Assessment . . . . .	70
6.3.3	Application Example: Bridge 547 (AKDOT) . . . . .	70
<b>Chapter 7 Conclusions and recommendations</b>	71	
7.1	Conclusions . . . . .	71
7.2	Recommendations . . . . .	71
<b>BIBLIOGRAPHY</b>	72	

## LIST OF TABLES

Table 2.1	Damage index level classification [65]	15
Table 3.1	Accelerated corrosion times in 3/4" rebar	30
Table 3.2	Corroded Rebar Test Matrix	35
Table 5.1	Design limit states	61
Table 5.2	Analysis matrix	64

## LIST OF FIGURES

Figure 2.1	Corrosion process in reinforcing steel bar [38] . . . . .	5
Figure 2.2	Concrete water to cement ratio vs rate of corrosion . . . . .	7
Figure 2.3	Diameter decrease due to corrosion . . . . .	7
Figure 2.4	Corrosion level vs time (years) . . . . .	8
Figure 2.5	Force displacement response of RC corroded columns [37] . . . . .	9
Figure 2.6	Corrosion process for RC column [37] . . . . .	10
Figure 2.7	Corroded rebars stress-strain curves [37] . . . . .	10
Figure 2.8	Strain aging effect on yield strength vs time (days) . . . . .	13
Figure 2.9	Park and Ang conceptual scheme . . . . .	14
Figure 2.10	Mainshock-aftershock sequence train of ground motions [49] . . . . .	18
Figure 2.11	Mainshock-aftershock sequence selection at T=0.4s for crustal earthquakes in Vancouver, British Columbia [57] . . . . .	19
Figure 2.12	Mainshock sequence selection at Eureka, CA [56] . . . . .	20
Figure 3.1	Rebar Specimen Geometry . . . . .	25
Figure 3.2	Rebars Ends Protection . . . . .	26
Figure 3.3	Large specimen containing three subset of specimens . . . . .	26
Figure 3.4	As received rebars anodic polarization immersed in pore solution for different times[18] . . . . .	28
Figure 3.5	Assembly for rebar preparation for the development of passive layer in pore solution . . . . .	28
Figure 3.6	Accelerated corrosion process . . . . .	29
Figure 3.7	Tension test setup example[44] . . . . .	31
Figure 3.8	BBT Test sequence[6] . . . . .	32
Figure 3.9	a) Picture of buckled bar; (b) Position of optical markers and adjustment to neutral axis; (c) Calculation of curvature [5] . . . . .	33
Figure 3.10	(a)Ductile rebar fracture; (b) Brittle rebar fracture [5] . . . . .	34
Figure 3.11	BBT results for rebars with and without ribs [5] . . . . .	34
Figure 4.1	Tension test setup and fracture observations . . . . .	38
Figure 4.2	Tension test results at different corrosion levels . . . . .	38
Figure 4.3	Yield strength as a function of corrosion level . . . . .	39
Figure 4.4	Yield strength as a function of corrosion level comparison of proposed model and Du et al model [13] . . . . .	40
Figure 4.5	Uniform elongation as a function of the corrosion level comparison of proposed model and Du et al model [13] . . . . .	41
Figure 4.6	General procedure of buckled bar tension (BBT) test . . . . .	42
Figure 4.7	Obtaining critical bending strain . . . . .	43
Figure 4.8	Bending strain at different corrosion levels . . . . .	44
Figure 4.9	Maximum bending strain as a function of corrosion level . . . . .	44
Figure 4.10	Basic features analysis of fracture surfaces in metals . . . . .	45

Figure 4.11 SEM observations for brittle and ductile failure at different positions of the fracture surface . . . . .	47
Figure 4.12 SEM cyclic loading features in fracture surface at 500x magnification . . . . .	48
Figure 4.13 Spectrum analysis of Back Scatter Electrons of fracture surface for brittle and ductile failures . . . . .	49
Figure 5.1 Corrosion modeling for structural analysis . . . . .	51
Figure 5.2 Uniform Hazard Spectrum for Anchorage, AK . . . . .	53
Figure 5.3 PSHA deaggregation for Anchorage, AK . . . . .	53
Figure 5.4 Mainshock selection from PEER NGA West2 database . . . . .	55
Figure 5.5 Mainshock-aftershock modeling for strain aging . . . . .	56
Figure 5.6 Structural Model a) SDOF Column b) Structural Model . . . . .	58
Figure 5.7 End point plastic hinge method [52] . . . . .	58
Figure 5.8 Section of the RC Column . . . . .	59
Figure 5.9 Force-Displacement results from experimental results [23] and analytical model . . . . .	62
Figure 5.10 Force-Displacement results from experimental RC column with corrosion in longitudinal bar (CL=9.5%) [31] and analytical model results (shown in lightblue) . . . . .	63
Figure 5.11 Strain hysteresis from experimental RC column with corrosion in longitudinal bar (CL=9.5%) results from analytical model . . . . .	63
Figure 5.12 Force-Displacement results . . . . .	65
Figure 5.13 Stress strain response for extreme rebar location . . . . .	66
Figure 5.14 CDF of steel yielding limit state using $IM = PGA$ . . . . .	67
Figure 5.15 CDF of steel yielding limit state using $IM = Sd(T_1)$ . . . . .	67

# Chapter 1

## Introduction

Structures are designed assuming their original condition remains intact through their service life. However, as structures age, they suffer various forms of degradation. In addition, they may be subjected to multiple discrete seismic events. Both of these items may impact structural performance. Consider an RC column and the limit state corresponding to bar buckling. The limit state displacement ( $\Delta$ ) to achieve bar buckling for a pristine column is different from a column subjected to corrosion. Similarly, multiple small seismic events may predispose the column to suffer longitudinal bar buckling for a lower level of seismic intensity. It is the goal of this research to incorporate both of these effects into the definition of performance limit states. This can potentially serve two purposes: a) for existing structures, assessment can consider likely current conditions, and b) for new structures, changes could be proposed to the initial design that could mitigate the effect of future condition degradation.

Structures subjected to multiple events and aging conditions should be considered in Performance-Based Earthquake Engineering (PBEE). Recent earthquake sequences such as the Christchurch 2010, Umbria-Marche Earthquake 1997 and more recently the Puerto Rico Earthquakes 2020, have shown that structures after sustaining damage during a mainshock have then collapsed or sustained increased damage after being subjected to a large magnitude aftershock[1][8][39]. Researchers have used the Park and Ang damage index (DI) to quantify damage, which is expressed as a two-term expression. The first term relates to the maximum displacement and the second term relates to the inelastic energy dissipation [65].The second term is associated with the inelastic cyclic behavior of structural components.In addition, the calibration factor is very small and contributes little to the damage index. If the damage index renders the inelastic cyclic behavior as negligible, it cannot accurately represent damage. Further, this damage index uses calibrated data to determine the strength degradation parameter that has a degree of

arbitrariness, which is undesirable [62]. In addition to the Park and Ang damage index, other measures of damage such as drift ratio based limit states have been incorporated into the PEER Performance-Based Design Probabilistic Framework[46][21][54]. The majority of these studies show that there is an increase in the probability of damage or even collapse of a structure due to repeated loading or aging conditions, such as high corrosion levels (CL). However, these results are based on the limitations presented by these damage measures [54]. In this study strain limits are used as indicators of damage for RC bridge columns. Specifically, concrete compressive and reinforcing steel tensile strain limits are used as damage measures [22]. These strain limits have been correlated to observed damage in large scale column tests. Therefore, we believe that our research will provide a realistic measure of the increase in damage for different limit states due to aging conditions and multiple earthquake loadings.

In addition, structures can have an existing condition such as corrosion that further deteriorates the performance of the structure. Corrosion is one of the aging conditions that more significantly deteriorates the seismic response of a structure. Thus, it is important to determine the limit states of corroded reinforcing steel. Currently, the literature has developed expressions that correlate the level of corrosion to the decrease in strength of the reinforcing steel[66][13]. However, these studies have utilized an accelerated corrosion process that does not consider the protective film that is developed on the reinforcing steel surface when it is embedded in concrete, a process known as passivation of the reinforcing steel [38][18]. For corrosion to occur, the protective film on the reinforcing steel bar must occur, this process is known as depassivation. Depassivation of the reinforcing steel greatly affects the behavior of reinforcing steel and can significantly modify the measured properties of the corroded reinforcing steel. Furthermore, no study has presented performance limit states on corroded reinforcement. Therefore, this research aims to close this gap by performing an experimental campaign. This experimental campaign consists of a series of tension tests and buckled bar tension tests to help define the performance limit states of corroded reinforcement. These results will then inform the computational model.

While corrosion is an important parameter that affects steel in structures, strain aging is a phenomenon that affects mild steels, which are common in older structures. Strain aging is the process in which steel after being subjected to large strains and an amount of time passes after the loading, when the steel is reloaded it presents a higher strength and reduced ductility than before the first loading. Therefore the incorporation of this parameter in this research will help evaluate this effect in older structures when subjected to repeated earthquake loading.

Moreover, there is a high likelihood for a structure in a high seismic region to be subjected to mainshock-aftershock sequence during its service life. Therefore, it is important to consider the effects of mainshock-aftershock sequences. A series of condition-dependent nonlinear time

history analyses are performed on a cantilever RC bridge column. The analysis applies a series of MS-AS sequence for different ages of the structure. The material properties of the structure are changed as a function of the aging conditions (e.g. corrosion). At the end of each analysis, the main variables of the study are the limit state that was reached, the controlling mode of response (flexural or shear controlled), the equivalent viscous damping, and the accumulated deformations.

In summary, this research aims to consider the likely future condition (considering deterioration mechanism and multiple earthquake loadings) of a structure in defining strain-based performance limit states.

## 1.1 Scope and layout

This research proposal describes the main components and objectives for the graduate studies of the author of this document. Chapter 2 contains the literature review which summarizes the state of the art in damage measurements and performance-based design framework. Chapter 3 covers the experimental campaign in corroded reinforcing steel. Chapter 4 summarizes the experimental and analytical procedures relevant to this study. Chapter 5 details the processing of current results.

# Chapter 2

## Literature review

Bridges are designed based on discrete events assuming that the initial material and structure properties remain constant through the life of the bridge. The purpose of the research described is to study condition dependent performance based design that considers the material and geometric properties as the structure ages, and the effects of multiple and discrete events on the achievement of prescribed limit states.

In this chapter, the current knowledge of aging of structures, damage indexes, corrosion and multiple earthquake loading is presented. Then the study gap and the objectives of this research are defined.

### 2.1 Corrosion

Corrosion is one of the main aging effects in RC structures. In RC structures after the concrete is cast a protective layer forms on the surface of the reinforcing steel, this process is known as passivation of the reinforcing steel. However, under conditions, such as chloride attack, the protective film can be broken, this process is known as depassivation. The depassivation process leads to corrosion. Corrosion reduces the area of steel, and also modifies the strength of the reinforcing steel. If corrosion degrades the structural performance of the reinforcing steel it will certainly degrade the overall strength of the system. The incidence of corrosion in RC structures in earthquake prone areas could trigger earliest onset of limit states, such as bar buckling or fractures (compared to pristine conditions). Therefore, it is important to incorporate the mechanics of corrosion in this condition dependent performance based seismic design. The general chloride attack corrosion process can be explained using three main parameters such as (1) time to initiation of corrosion, (2) corrosion growth in reinforcing steel, and (3) the

mechanical properties of corroded reinforcing steel. Figure 2.1 schematically shows the corrosion process.

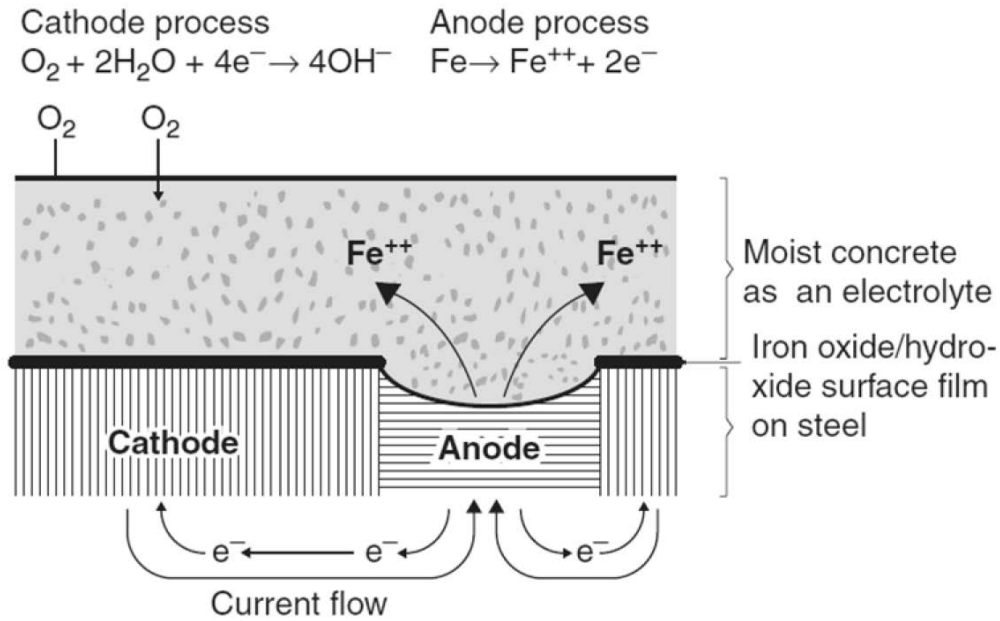


**Figure 2.1** Corrosion process in reinforcing steel bar [38]

### 2.1.1 Time to corrosion

Jensen et al performed a series of experiments to measure the chloride ingress in the cement and mortar paste [26]. In their study, it was determined that the ingress of chlorides follows Fick's law of diffusion, shown in Eq. 2.1. Stewart et al solved Eq. 2.1 in terms of the chloride ion concentration ( $C(x, t)$ ), distance from concrete surface ( $x$ ), time of exposure to chloride ions ( $t$ ), and the chloride diffusion coefficient ( $D_c$ ). The solution rendered equation Eq. 2.2 which describes the time to initiation of corrosion [55][63][58]. Mean values for  $C_0$  and  $C_r$  have been previously defined for environments that are controlled by deicing salts [20][61][14].

$$\frac{\partial C(x, t)}{\partial t} = D_c \frac{\partial^2 C(x, t)}{\partial x^2} \quad (2.1)$$

$$T_{corr} = \frac{x^2}{4D_c} \left[ erf^{-1} \left( \frac{C_0 - C_{cr}}{C_0} \right) \right]^{-2} \quad (2.2)$$

### 2.1.2 Rate of corrosion

Vu et al developed an empirical model to evaluate the corrosion rate [60][55]. In their study a constant corrosion rate was assumed. However, it is known that the corrosion rate is not constant over time because it is dependent on factors such as the quality of concrete, the amount of oxygen available in the environment, and the relative humidity. Nonetheless, for long term studies this approximation is valid. The underlying assumptions of this model are a relative humidity of 75% and a temperature of 20°C. The model developed by Vu et al is shown in Eq. 2.3. Figure 2.2 shows the corrosion rate for different concrete covers ( $d_c$ ), as a function of the water to cement ratio ( $w/c$ ). In general, for large values of cover depth the rate of corrosion decreases rapidly, and as the water to cement ratio (i.e. lower quality concrete) increases the rate of corrosion increases.

$$i_{corr} = \frac{37.5(1 - w/c)}{d_c} \quad (2.3)$$

In addition, Vu et al further improved the model of corrosion growth in reinforcing steel developed by Stewart et al [60][55][10][20]. Their proposed model describes the reduction in diameter of reinforcing steel ( $d_{corr}(t)$ ) as a function of time described in Eq. 2.4. Figure 2.3 shows this model applied to a rebar with an initial diameter ( $d_{bi}$ ) of 3/4 inch, a concrete cover of 1-1/2", and water to cement ratios ranging from 0.36-0.50.

$$d_{corr}(t) = d_{bi} - \frac{1.0508(1 - w/c)}{d_c} (t - t_{corr})^{0.71} \quad (2.4)$$

Further, the evolution of corrosion in reinforcing steel can be expressed in the percent loss of mass of a rebar. If uniform corrosion is assumed, this can be expressed as the percent of reduction of diameter. The corrosion level can be expressed as shown in Eq. 2.5.

$$CL = \frac{d_{bi} - d_{corr}(t)}{d_{bi}} * 100 \quad (2.5)$$

Combining Eq. 2.4 with Eq. 2.5, the variation of the corrosion level can be described as a function of time. Figure 2.4 shows the results of this process.

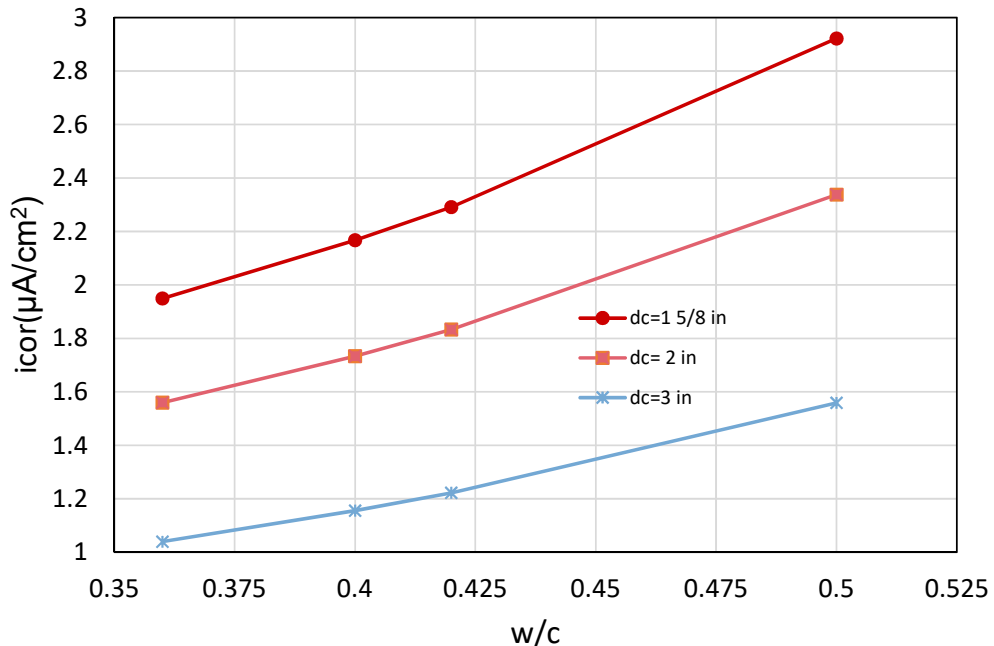


**Figure 2.2** Concrete water to cement ratio vs rate of corrosion

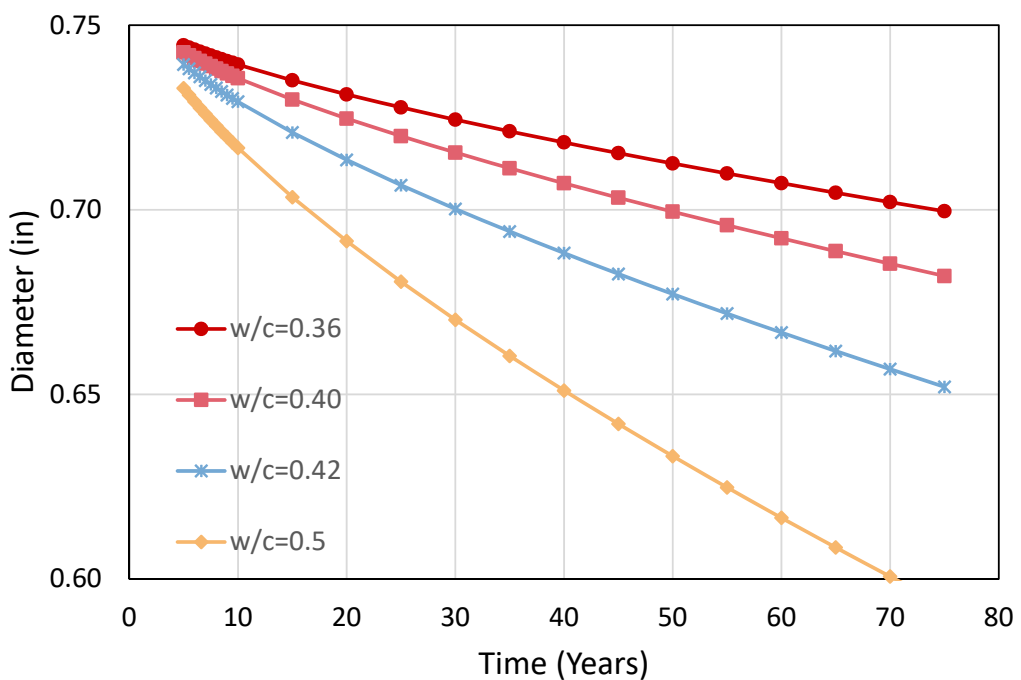


**Figure 2.3** Diameter decrease due to corrosion

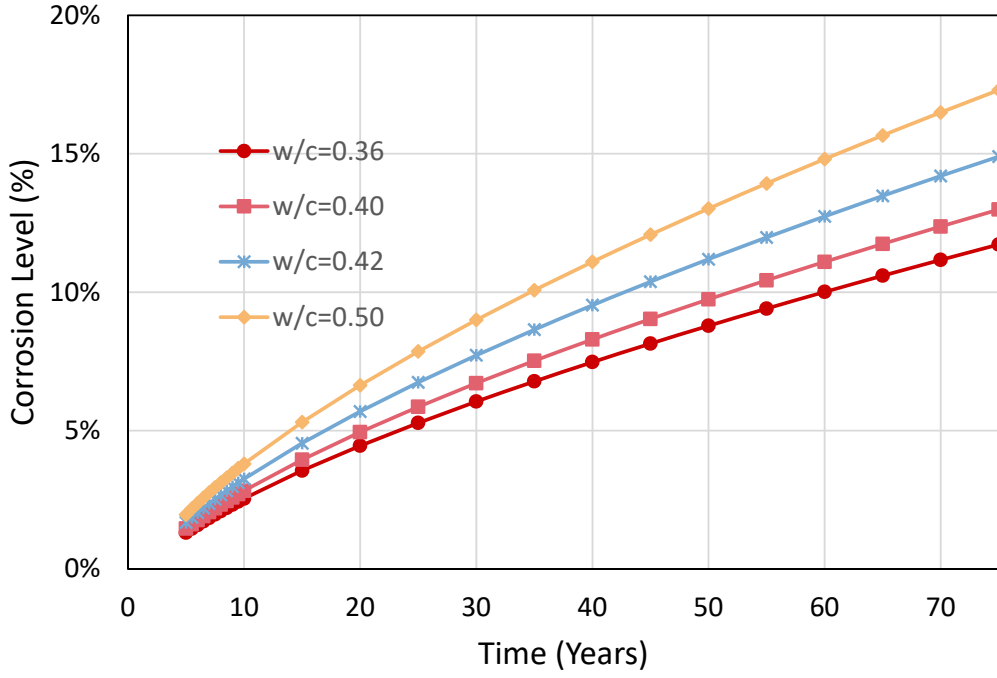


**Figure 2.4** Corrosion level vs time (years)

### 2.1.3 Corrosion modified properties of reinforcing steel bars

Yuan et al [66] performed tension tests on corroded rebars and determined that the mechanical properties of steel change with the level of corrosion. In general, as corrosion increases, the yield strength and ultimate strength of the reinforcing steel decrease. The variation of the mechanical properties is shown in Eq. 2.6 for the yield strength and ultimate strength of the reinforcing steel.

$$f_{y,CL} = f_{yo}(1 - 0.021CL) \quad (2.6)$$

$$f_{u,CL} = f_{uo}(1.018 - 0.019CL)$$

One of the limitations in their study is that the accelerated corrosion process used to develop the corrosion in the rebars did not account for the depassivation process that naturally occurs in rebars embedded in concrete. Chapter 3 shows a proposed experimental assessment that will provide an accurate evaluation of the mechanical properties of corroded reinforcing steel.

#### 2.1.4 Physical test on corroded RC Structures

Recent studies [31], [37] and [64] have been developed to assess the effect of corrosion in the structural performance of cantilever RC columns. These columns were subjected to accelerated corrosion to obtain different corrosion levels ( $CL$ ). The range of  $CL$  for these studies correspond to  $CL = 0\% - 20\%$ . In these studies the accelerated corrosion was performed via an electrochemical process directly applied to the reinforcing steel as shown in Fig. 2.5.

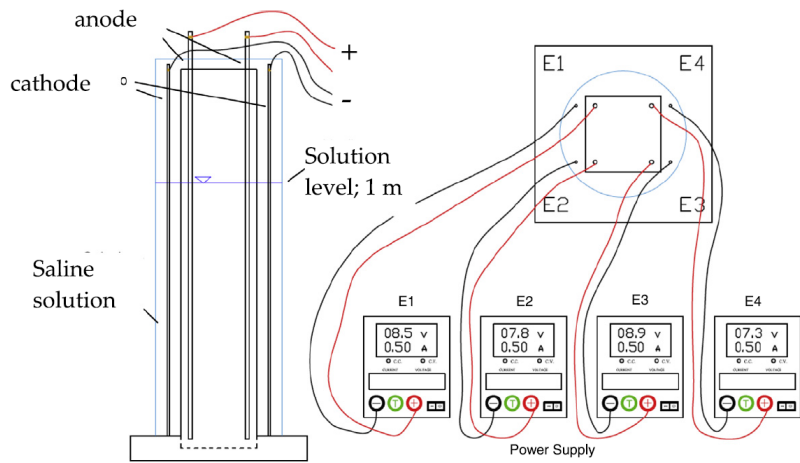


**Figure 2.5** Force displacement response of RC corroded columns [37]

The corroded RC columns where then subjected to a quasi-static loading protocol. The resulting force displacement response of one of these experiments is shown in Fig. 2.6. It can be seen that there is a reduction of he strength and displacement capacity of the system.

As stated in the previous section the mechanical properties of steel are affected by corrosion. In the previous studies [37] the authors performed tension tests on corroded reinforcing steel. In these tests a reduction in the mechanical properties of steel was observed as well as a reduction in the rupture strain  $\varepsilon_{srup}$ , see Fig. 2.7.

While these studies show how corroded RC columns behave under cyclic loading, they did not consider the generation of the protective film due to the alkaline environment of the concrete. This film can modify the mechanical properties of corroded steel. In addition, the accelerated corrosion process used a 3%  $NaCl$  concentration solution while the chloride attack in concrete usually has a 1.0% - 1.5% concentration of the same chloride. Therefore the results obtained from these studies do not accurately represent the actual conditions of corroded RC columns. Thus,

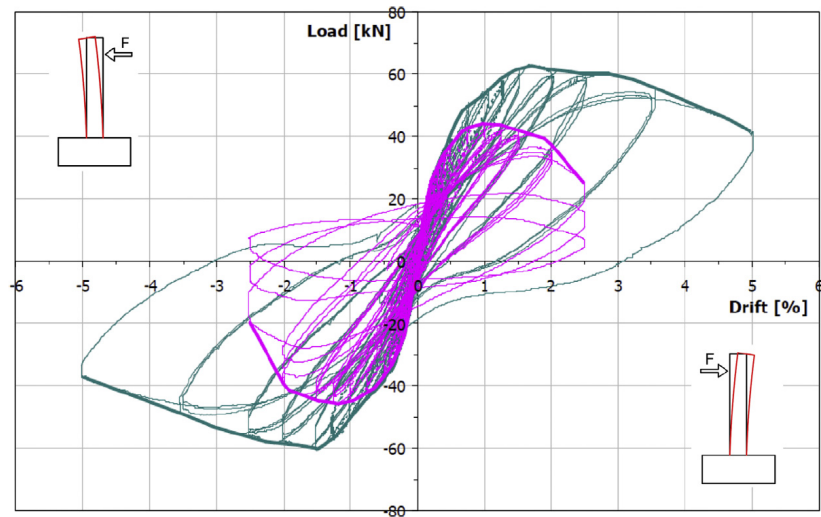


**Figure 2.6** Corrosion process for RC column [37]

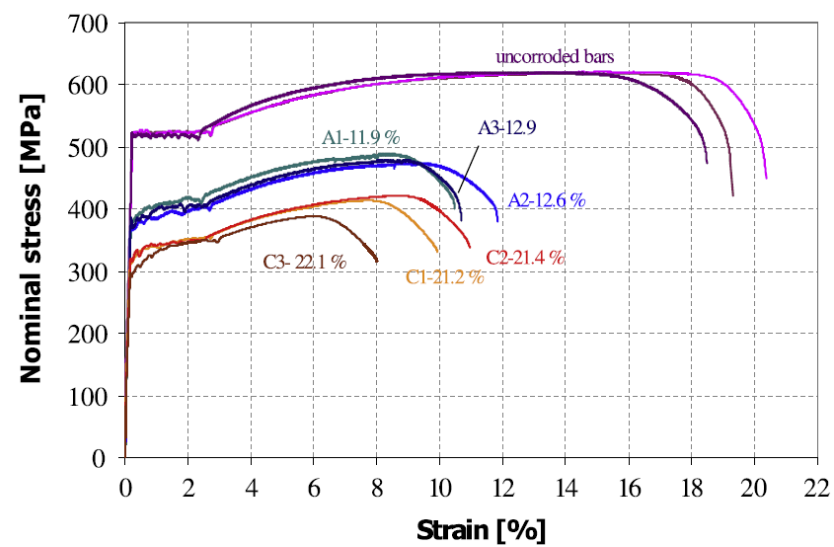


**Figure 2.7** Corroded rebars stress-strain curves [37]

an experimental campaign is proposed that will provide results on the mechanical behavior of corroded reinforcing steel inside concrete. The experimental campaign is discussed in Chapter 3.

## 2.2 Steel strain aging

While corrosion is an important parameter that affects steel in structures, strain aging is a phenomenon that affects mild steels, which are common in older structures. Strain aging is the process in which steel after being subjected to large strains and an amount of time passes after the loading, when the steel is reloaded it presents a higher strength and reduced ductility than before the first loading. Therefore the incorporation of this parameter in this research will help evaluate this effect in older structures when subjected to repeated earthquake loading. This process is explained in more detail in this section.

### 2.2.1 Metallurgical process

It is generally accepted that strain aging is due to the diffusion of carbon and/or nitrogen atoms in solution to dislocations that have been generated by plastic deformation. Initially, an atmosphere of carbon and nitrogen atoms is formed along the length of a dislocation, immobilizing it. Extended aging, however, results in sufficient carbon and nitrogen atoms for precipitates to form along the length of the dislocation[45][25].

These precipitates impede the motion of subsequent dislocations and result in some hardening and loss in ductility. The extent of strain aging, which is a thermally activated process, depends primarily on aging time and temperature. In general, extended aging results in a saturation value above which further aging has no effect [50].

A second strengthening mechanism occurs when cold deformation (alone) is applied to steels. When dislocations break away from their pinning interstitial atoms and begin the movement causing slip they begin to intersect with each other. A complex series of interactions between the dislocations occurs, causing them to pin each other, decreasing their mobility. The decreased mobility also results in higher strength, lower ductility and lower toughness. As a result, cold deformed steels already have lowered ductility and toughness before any strain aging occurs. When heating follows cold deformation, the loss in ductility and toughness is greater. It is this combination of events that is the most damaging to the toughness of structural steels [40].

### 2.2.2 Strain aging effects in structures

Strain aging is the process by which steel after being subjected to large strains, develops an increased strength and reduced ductility with time. Large earthquakes can cause this effect on structures built with mild steel. Therefore, it is important to include strain aging in a time dependent analysis. Furthermore, strain aging will cause an increase in the strength of the plastic hinge and as a consequence plastic hinges may form in regions of the structures that have not been designed for such demands. The effects of strain aging may also alter the transverse reinforcement due to cold bending, making them susceptible to brittle failure[40].

According to Restrepo-Posada[50], most strain aging occurs in the first 37 days. In addition, Momtahan et al [40] studied strain aging effects with respect to time at different levels of pre-strains. The pre-strains ranged from  $2\varepsilon_y$  to  $10\varepsilon_y$ , for a time frame of 3 days to 50 days. Their results determined that a significant effect of strain aging took place from pre-strains  $5\varepsilon_y$  and on. Strains higher than  $15\varepsilon_y$  indicate a performance level in which substantial damage has been induced in the structure such that it is deemed unrepairable and therefore pre-strains higher than  $15\varepsilon_y$  are impractical and were not studied [40].

Momtahan et al correlated the increase in yield strength as a function of time and the pre-strain in reinforcing steel bars. The proposed equations are shown below:

For  $10\varepsilon_y$

$$\frac{f_y}{f_{yi}} = 0.0026t + 0.9838 \quad (2.7)$$

For  $5\varepsilon_y$

$$\frac{f_y}{f_{yi}} = 0.0008t + 0.996 \quad (2.8)$$

For  $2\varepsilon_y$

$$\frac{f_y}{f_{yi}} = 0.0004t + 0.9979 \quad (2.9)$$

It is proposed to limit the increase in yield strength obtained at 50 days, which was the limit of scope of their study. Equations 2.7 to 2.9 are plotted in Fig. 2.8

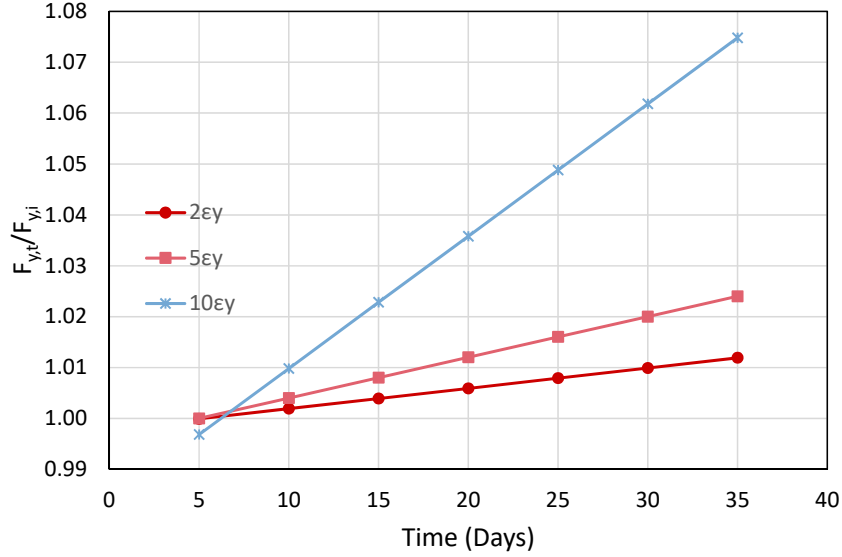


**Figure 2.8** Strain aging effect on yield strength vs time (days)

## 2.3 Damage Indexes

The use of damage indexes has dominated the research related to damage accumulation. While these methods are practical, in the sense that they can be easily deployed in probabilistic analyses, and appear to have a logical basis, they are based on empirical relationships and need to be correlated for each structure case to be of any significance. An example is shown in this section demonstrate this inconsistency. The literature review presented here is to understand what has been done previously to study the effect of damage accumulation, however it is the purpose of this research that strain limit states are an improved measure of damage over empirical methods.

The effect of cumulative damage in structures was studied by Park and Ang (1985) [65] in their study the authors proposed the damage index as shown in Eq. 2.10. The damage index was used as a measure to quantify damage in terms of the maximum experienced earthquake and the absorbed hysteretic energy.

$$D = \frac{\Delta_m}{\Delta_u} - \beta \frac{E_h}{F_y \Delta u} \quad (2.10)$$

$\Delta_m$ : Maximum deformation under earthquake

$\Delta_u$ : Ultimate deformation under monotonic loading

$F_y$ : Calculated yield strength

$E_h$ : Total hysteretic energy

$\beta$ : Dimensionless constant

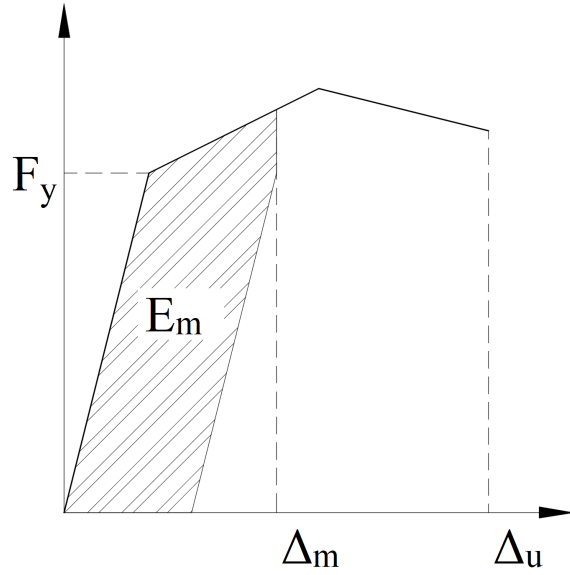


**Figure 2.9** Park and Ang conceptual scheme

Equation 2.10 was derived for concrete elements. The first term here is a simple, pseudo-static displacement measure. The second term accounts for cumulative damage. This concept is shown in Fig. 2.9. The advantages of this model are its simplicity and flexibility in adapting the model to correlate with experimental data. After calculating the damage index, this can be classified according to the damage index level defined by Park and Ang [65]. The damage index level classification is shown in Table 2.1.

However, this model has several limitations. Firstly, the calibration of the  $\beta$  coefficient with observed damage has proven to be very low ( $\beta = 0.05 - 0.15$ ) [65] [21], rendering the second term relatively inconsequential compared to the contribution of the first term. A sample result is taken from Gosh et al [21], which applied a modified version of the Park and Ang damage index in terms of the moment ( $M_y$ ), the rotation ( $\theta_y$ ), and curvature ductility ( $\mu$ ). The modified model is expressed in Eq. 2.11.

**Table 2.1** Damage index level classification [65]

Level	Damage index (DI)	Damage measure
I	DI<0.1	No damage; localized minor cracking
II	0.1<DI<0.25	Minor damage; light cracking throughout
III	0.25<DI<0.4	Moderate damage; severe cracking; localized spalling
IV	0.4<DI<1.0	Severe damage; crushing of concrete; reinforcement exposed
V	D>1.0	Loss of elemental load resistance

$$D = \frac{\mu_m}{\mu_u} - \beta \frac{E_h}{M_y \theta_y \mu u} \quad (2.11)$$

Using the following values:  $\mu_m = 4.93$ ;  $\mu_u = 17.02$ ;  $M_y = 8751.375$ ;  $\theta_y = 0.0042$ ;  $E_h = 119.07$ ;  $\beta = 0.05$

And substituting in equation Eq. 2.11:

$$D = \frac{\mu_m}{\mu_u} - \beta \frac{E_h}{M_y \theta_y \mu u} = 0.3$$

**First term:**

$$\frac{\mu_m}{\mu_u} = \frac{4.93}{17.02} = 0.2897$$

**Second term:**

$$\beta \frac{E_h}{M_y \theta_y \mu u} = 0.05 \frac{119.07}{8751.375 * 0.0042 * 17.02} = 0.0103$$

It can be seen that 97% of the damage index comes from the first term, which is the elastic term, and the inelastic part is only 3% of the total.

Despite its limitations, several studies have used or modified this model to study the effects of cumulative damage for different structures. Those of relevant importance are those performed by Kunnath et al [30], who used a modified Park and Ang model, to account for damage at the local level for elements in the structural analysis program IDARC 3.0. In this software, for the case of multiple degrees of freedom buildings they also added parameters to consider the damage at the inter-story level and the global model. Ghosh et al [21] developed a damage accumulation framework to estimate the probability of exceeding a damage index for multiple ground motions. Other regressions have been proposed [27], [15], [51] but show no improvement in assessing the damage state of a structure. While these studies provide an insight into some of the characteristics of damage accumulation they, still rely on the Park and Ang model and therefore carry the same limitations.

Krawinkler (1987) [28] proposed a method that considered damage as a function of low cycle fatigue parameters. The form of the Krawinkler damage index for steel components, weldments, and local buckling has a general shape of the Miner model. This model relies on the accumulation of plastic deformations. While this model has proven to work well for the evaluation of individual steel structure elements, it does not provide a way to generalize damage for other types of structures.

## 2.4 Multiple earthquake loading

The evaluation of multiple seismic events has been scarcely studied; however, their effects have been felt in numerous earthquake sequences such as the Christchurch 2010, Umbria-Marche Earthquake 1997 and the Puerto Rico Earthquakes 2020. The hypothesis is that accumulation of damage will restart in a smaller seismic event to achieve a prescribed limit state, similar to how corrosion and other aging phenomena might impact the intensity needed to achieve a future limit state.

In the literature the study of multiple earthquake loading can be classified in two groups:

- Mainshock-aftershock sequences
- Mainshock sequences

These studies have shown what are some of the effects of multiple earthquake loading for different structures.

### 2.4.1 Mainshock-aftershock sequences loading

Strong aftershocks can increase the state of damage of a building or even collapse an already damaged structure. It is therefore important to quantify the increase of seismic demands in structures due to aftershock loading. In recent years different studies have been carried out to develop methodologies that consider these effects.

Tesfamariam et al [57] investigated the increase in the demands for multiple degrees of freedom systems (MDOF). They conducted a parametric study of RC bare frame buildings and RC frame with infill masonry buildings. The main parameter of study focused on the thickness of the infill frames ranging from 75mm - 125 mm. In addition, a series of mainshock-aftershock sequences were applied, selected for the area of Vancouver, BC. The mainshock-aftershock sequence were selected using the conditional mean spectra (CMS) over the period range of the structures. The motions considered in their study were different for the bare frame and

the infill frames. The bare frame was subjected to a mainshock followed by three aftershocks, while those of the infill frame consisted of one mainshock followed by one aftershock each. Their results showed that there is an increase of 10% in the inter-story drift demands for the RC bare frame structures. For the case of infill frames the inter-story drift did not significantly increased. Their study used FEMA 356 [16] to define the performance limit states. FEMA 356 drift performance limit states are based on linear regression on observed damage to drift level obtained from experimental tests. The linear regression compared to the experimental results have high dispersion. Therefore, it is possible that in the study by Tesfamariam et al, that while a drift limit state did not increase after applying a MS-AS sequence, a higher strain was reached in some of the components due to the MS-AS sequence, and as consequence a higher strain performance limit state could have been reached. Thus emphasizing the importance of using strain performance limit states. Similarly, Raghunandan et al [49] studied the vulnerability of RC frame structures. Their study showed that depending on the level of interstory drift achieved during the mainshock the additional damage experienced during the aftershock will be different. For example, the authors showed that for an RC frame that experiences 4% or more interstory drift in the mainshock, the median capacity to resist aftershock shaking is reduced by about 40%. Furthermore, other studies have focused on the behavior of single degree of freedom (SDOF) systems response to mainshock-aftershock (MS-AS) sequences [24][34]. Hatzigeorgiou et al focused on determining the inelastic displacement coefficient variation due to the MS-AS sequence. Their study concluded that there is an increase in the inelastic displacement demands, however, the limitations in their study did not report what happens to the performance limit states. Further, Manafpour et al studied the seismic drift behavior of structures to MS-AS sequences for far-field earthquakes and near-field earthquakes. Their study concluded that for SDOF structures near-field earthquake sequences were the most damaging, increasing the drifts by as much as 45% compared to a structure subjected to the main shock only.

Researchers have applied two earthquake selection procedures for mainshock-aftershock sequences. The first method, incremental dynamic analysis (IDA), consists of 1)subjecting the nonlinear building model to a ground motion having a particular intensity, 2) recording the response of the structure [59], 3)in successive analyses, the ground motion is incrementally scaled to a higher intensity measure (IM), and 4)the structural response is recorded in each analysis. The IDA procedure was extrapolated to for MS-AS sequence as follows: 1)Apply the IDA to the mainshocks to obtain 11 drift damage levels ranging from 0.5% to 5.5% of interstory drift in the structure, 2) after each mainshock include an incrementally scaled aftershock with a 4 seconds gap between the mainshock and the aftershock, and 3)Change the polarity of the aftershock, which refers to the direction of the aftershock variation to the mainshock. Fig. 2.10 shows one of

the resulting MS-AS sequences using the IDA methodology. Due to the use of scaling factors the IDA methodology uses artificial mainshock-aftershock sequences. In addition, the IDA analysis can be computationally expensive. For instance, the authors reported a total of 9900 ground motion sequences per structure.

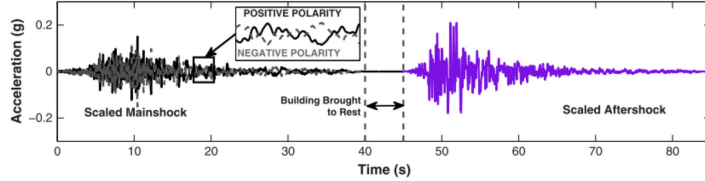


**Figure 2.10** Mainshock-aftershock sequence train of ground motions [49]

The second method consists of matching the MS-AS sequences to a site seismic hazard curve obtained from a probabilistic seismic hazard analysis (PSHA). Tesfamariam [57] used conditional mean spectra (CMS) to match and select mainshock-aftershock sequences for structures located in Vancouver, BC. Their study selected MS-AS sequences from two databases of ground motions, NGA-West2 [2], and the K-NET//KiK-net [42]. The CMS process consists of computing the expected response spectrum associated with a target spectral acceleration ( $S_a$ ) value at a single period, using the known values from the PSHA such as the magnitude, distance, and  $\epsilon$  values. In their study the authors used CMS to select the MS-AS sequences for different earthquake scenarios a)Crustal earthquake, b) Interface, and c) Inslab. They hypothesized that different earthquake scenarios would have different MS-AS sequence characteristics such as higher spectral acceleration ( $S_a$ ) values at short periods for interface earthquakes, and high  $S_a$  values at longer periods for crustal earthquakes. They argue that using the CMS method makes the selection of ground motion consistent with the seismological features of the area of study. Fig. 2.11 shows this selection for a structure with a 0.4s period for crustal earthquakes. The CMS method adapts to the site conditions, no scaling of MS-AS is required since the selection is optimized to ground motion sequences stored in the databases. Since the CMS method uses site-specific data, it can be a part of an analytical framework that can be adapted to different seismic regions.

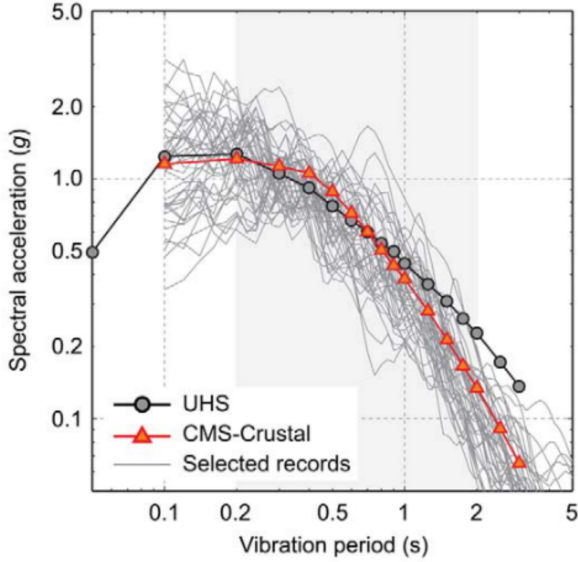


**Figure 2.11** Mainshock-aftershock sequence selection at  $T=0.4\text{s}$  for crustal earthquakes in Vancouver, British Columbia [57]

#### 2.4.2 Mainshock sequences loading

Reliable temporal prediction of earthquakes is currently impossible. However, for a large region, earthquakes recurrence time can be modeled reasonably well as a Poisson process. Sunasaka [56] developed mainshock sequences that followed a Poisson process. Their study focused on the accumulation of damage due to mainshock sequences, and mainshocks-aftershocks sequences. Damage accumulation was accounted for by the Park and Ang index. The authors used ground motion prediction equations to develop artificial mainshock sequences. Their study calculated the recurrence period, magnitude, location and peak ground acceleration for each of the mainshocks. The author subjected an SDOF bridge in Eureka, CA to the mainshock sequence shown in Fig. 2.12. While the results shows a significant increase in the damage index due to mainshock sequences, the conclusions are limited by the assumption that a Poisson process can be applied to single faults, which has not shown good correlation with observed events[53]. While this study shows what could be possible if mainshocks were predictable in small regions, more advances in seismology are needed to confidently apply the proposed methodology.

Other studies have used three equally spaced mainshocks [24]. The three equally spaced mainshocks can be deployed without much computational effort, however, there is not a seismological basis for the use of three equally spaced mainshocks. Therefore, the use of this method-

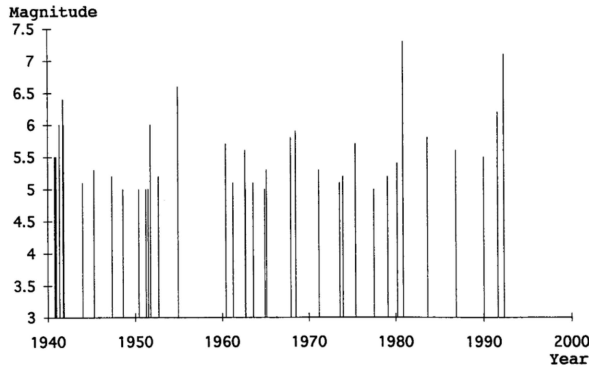


**Figure 2.12** Mainshock sequence selection at Eureka, CA [56]

ology would be limited to a scenario analysis and not useful for analysis and design, since the probabilities of three equally spaced in time mainshocks on any given structure is very low.

## 2.5 Aging of structures

There have been attempts by many researchers to characterize the aging of structures.

In recent years studies have focused on the effect of cumulative damage. These studies have focused on assessing the damage accumulation considering multiple earthquakes, corrosion and service life of the structure. Two field of study have been observed:

- Probabilistic framework
- Fragility curves

### Probabilistic Framework

One of the most widely used probabilistic frameworks is the Pacific Earthquake Engineering Research Center (PEER) Performance Based Design (PBD). PEER PBD can be expressed by the following equation:

$$\nu_{DM}(dm^{LS}) = \iint D_{DM|EDP}(dm|edp)|, dG_{EDP|IM}(edp|im)|| d\nu_{IM}(im)| \quad (2.12)$$

Mackie et al [32] using the PEER PBD, developed the performance based damage design (PBDD) and performance based loss design (PBLD) by defining the probabilistic demand, damage, and loss model parameters in terms of reinforced concrete column damage. The RC

column damage was defined in terms of mean drift ratios obtained from the PEER structural performance database (<http://nisee.berkeley.edu/spd/>). The drift limit states considered in their study were concrete spalling, bar buckling and failure. In their study, failure was defined as the first occurrence of the database fields for reinforcing bar fracture and loss of axial load-carrying capacity.

The authors show that for a given intensity measure (*IM*) and a confidence level of achieving a limit state, it is possible to then define the probability of exceeding that limit state. The authors used peak ground velocity (*PGV*) as their intensity measure. While this methodology was able to define damage and incorporate it into the PEER PBD framework, the authors did not consider strain to define the limit states. In a PEER report Mackie et al studied seismic demands for performance-based design of bridges. In the report they performed a design parameter sensitivity analysis in which they evaluate different intensity measures. Their analysis showed that the optimal *IM* to predict most engineering demand parameters (*EDP*) is the first mode spectral displacement  $S_d(T_1)$  [33]. However, at the time their report was written the  $S_d(T_1)$  did not show good correlation with strain as the *EDP*, and as a consequence they did not recommend to use strain as a predictor of structural performance. Nonetheless, a recent study presented by Krish et al shown that new advancements in the modeling of plastic hinge forming members can more accurately relate strain and  $S_d(T_1)$ . They conclude that the use of these parameters is well suited to predict the performance of structures [29].

### **Fragility Curves**

Another common trend in this subject is the use of fragility curves to estimate the effect of damage in structures. Two main approaches were found in the literature. One of them relied on the Park and Ang Model damage index to define damage, while the second approach related damage to drift.

Ghosh et al [21] formulated a damage accumulation framework. Their study relied on the Park and Ang Damage index explained in the previous section. The study performed a series of nonlinear time history analyses for two cases:

- Using a constant main shock hazard occurrence rate (3 main shocks in a 50-year period)
- Mainshock - Aftershock series using a time-dependent aftershock hazard occurrence rate

The results from their study showed regression equations that statistically predict the damage index as a function of earthquake intensity and damage history. This study revealed that for both mainshock and aftershock scenarios there was a significant increase in the probability of damage index exceeding a damage index level (as defined in Table 2.1) under repeated shock

scenarios. While this study shows the importance of considering damage accumulation, these results have to be taken with caution, since they present the same disadvantages as the Park and Ang damage index.

Ghosh et al [20] also studied the effects of corrosion on time dependent seismic fragility curves. Their study characterizes corrosion in concrete columns as a continuous phenomenon that occurs as a function of time. The authors also considered the effects of corrosion on steel bridge bearings. The authors then ran a series of NLTHA analyses for different aging times of the structures. Based on their analysis, time dependent fragility curves were presented. The results showed that as time increases, and corrosion increases as a consequence, the probability of exceeding a limit state increases. In their study, limit states were defined on the basis of inter-story drifts which were obtained from experimental results and field observations [46]. It is important to mention that the limit states used in their study were not defined on the basis of strains or other structural property. Instead the limit states came from a survey performed in central and southeastern United States departments of transportation, on the premise of a range of experienced inter-story drifts and the time taken to repair them. In addition, assuming that corrosion is a continuous process has to be cautiously taken as valid. This is because site information such as temperature, water to cement ratio, the addition of cementitious materials such as silica fume, and the environment (e.g. coastal vs inland) affect the rate of propagation of corrosion[58].

While these studies provide a general view on how damage increases the likelihood of observing collapse or deterioration of the seismic performance, the methods used to arrive at those conclusions can be misleading since the definition of damage as either a Damage Index or Drift are not the best parameters to quantify the damage. It is our belief that strain-based limit states will provide a better understanding of the implications of damage accumulation.

## 2.6 Research Gap

Many studies have tried to show the importance of quantifying the effects of accumulated damage and multiple shocks throughout the lifetime of a structure. Therefore, it is important to develop a model that establishes the likelihood of achieving a limit state as the structure ages. In addition, it is important to understand the impacts of aging on bridge seismic performance. Furthermore, bridges in seismic areas can be subjected to main shock and aftershocks. Therefore, a methodology that incorporates both aging and multiple seismic events is needed.

Damage accumulation is a topic that has been gaining momentum in the engineering community, this study will better inform the potential future conditions of a structure to stakeholders

such as state DOTs, building owners, and practicing engineers. In the literature it was observed that damage accumulation has been studied using the Park and Ang damage index or drift-based limit states to measure damage accumulation. Different researchers have also included corrosion into their scope of analysis, which shows that aging conditions play an important role in the deterioration of a structure. In addition, Krish [29] determined that spectral displacement at first effective period is an improved intensity measure (IM), while the past literature used the peak ground acceleration (PGA) as the controlling IM. This research will develop a parametric study using a series of single degree of freedom (SDOF) systems, subjecting them to different conditions such as corrosion, and steel strain aging. The SDOF structures will be subjected to a sweep of ground motions using nonlinear time history analysis to obtain maximum strain demands. With the results from NLTHA, fragility functions will be used to show the increase in the likelihood of reaching a performance limit state due to aging of the structure. In addition, this research will provide the engineering community with a design framework to account for damage accumulation in their analysis and guide decisions on the resiliency of a structure. In addition, this study will provide a methodology in which the Direct Displacement-Based Design (DDBD) is modified to consider the effects of damage and aging conditions.

### 2.6.1 Objectives

The main goal of this research is to provide a design methodology to consider damage for performance based seismic design of structures. In addition, this study will demonstrate the implications of aging conditions and multiple earthquakes for the design of bridge RC columns.

- Incorporate different aging conditions and develop fragility curves that considers strain limit states as a measure of damage
- Establish limit states for corroded rebars
- Describe the methodology to appropriately mimic real corrosion process in material experiments of corroded rebars, which can later be extrapolated to large scale testing of RC columns subjected to corrosion
- Consider the effects of multiple earthquakes for two cases: (1) Mainshock-Aftershock sequence, and (2) Mainshock-Aftershock sequence with the effects of time (corrosion and strain aging) between the mainshock and the aftershock.
- Incorporate these results into the Direct Displacement Based Design (DDBD) methodology.

## Chapter 3

# Experimental program: mechanical properties and performance of corroded rebars

Corrosion is the main aging condition that affects structures. Therefore, the success of this study relies on the most accurate representation of the corrosion process in the analytical model. As mentioned in Chapter 2, previous studies developed accelerated corrosion rebar specimens with high current densities, but did not account for the depassivation process of the reinforcing steel. A main objective of this study is to verify the mechanical properties of corroded rebars while considering the depassivation process in rebars. The experimental process is divided in to three main components, (1) generate the passive layer in rebar specimens, (2) depassivate and corrode the rebar specimens, and (3) obtain the mechanical properties of the reinforcing steel by performing tension tests and buckled bar tension (BBT) tests. It is expected that these tests will mimic as best as possible the real aging conditions of rebars inside a concrete mix. The results obtained from the tension and BBT tests will be used to update the analytical model presented in Chapter 5, and more broadly provide accurate mechanical properties of corroded rebars.

### 3.1 Proposed experimental campaign

Rebars embedded in concrete generate a protective film that protects the rebars against corrosion, due to the alkaline environment of the cement paste. The most common form of corrosion occurs via chloride attacks. During a chloride attack, the chloride diffuses in the concrete cover

and enters in contact with the surface of the rebars. This initiates the process of depassivation in which the protective film on the surface of the rebar is eliminated. The depassivation of the rebar enables the process of corrosion to occur. The proposed experimental campaign described in this chapter aims to simulate the process of corrosion as it would occur in rebars embedded in concrete. Using as received rebars, that is no special treatment to the surface of the rebar, the tests procedure consist of (1) protect the rebar ends that will be used as grips during the tension and perform buckled bar tension (BBT) tests, (2) generate the passive layer on the rebars, (3) perform accelerated corrosion of the rebars until the specified levels of corrosion, (4) perform tension tests to characterize the tension stress-strain behavior of corroded rebars, and (5) perform the BBT tests that will provide data on the ultimate limit state of corroded rebars. The different procedures of the experimental campaign are further explained below.

### **Preparation of rebar ends**

First, it is necessary to protect the areas of the rebar that are going to function as grips for the rebars during the tension and BBT tests against corrosion. Therefore, the ends of the rebars will be protected with three layers. The first layer consists of two-part epoxy, the second layer consists of electroplater tape, and the third layer consists of shrink tube. These layers will ensure minimal corrosion in the grip areas of the rebar. Fig. 3.1 and Fig. 3.2 show the specimen geometry and the protective layers at the ends of the rebars.

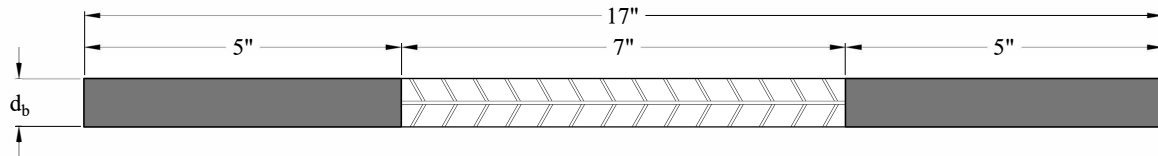


**Figure 3.1** Rebar Specimen Geometry

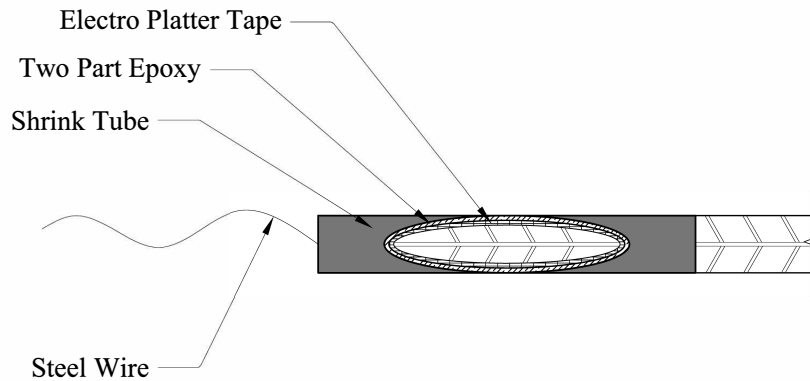


**Figure 3.2** Rebars Ends Protection

To optimize the space and time it takes to prepare the rebars for corrosion, a large rebar that contains three specimens will be prepared. This ensures that the large specimen, which will be placed in a corrosion cell, provides the same level of corrosion to all the specimen subsets. After each large specimen has the specified level of corrosion, the large specimen will be cut into the three smaller specimens shown in Fig. 3.1.

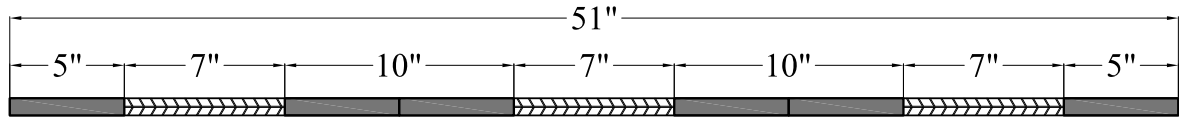


**Figure 3.3** Large specimen containing three subset of specimens

### **Passivation of the rebars**

In order to simulate the conditions of rebars embedded in concrete, it is necessary to generate the passive layer on the surface of the rebars. There are two ways to generate the passive layer: (1) embed rebars in concrete and wait for the passive layer to generate, or (2) submerge the reinforcing steel in a synthetic pore solution that mimics the cement paste environment. The second option is more suited for material testing since it does not involve demolishing the concrete. To this regard, Ghods et al [19] developed ten different pore solutions to generate the passive film on the surface of rebars. The pore solutions that were developed in their study intended to mimic the cement paste. Their study conducted 10 solutions designed to encompass concentrations of  $Ca^{+2}$ ,  $Na^+$ ,  $K^+$ , and  $(SO_4)^+$  found in the cement paste. The solution that generated the passive layer with the best quality of protective film will be used in this study. To achieve the desired concentration of the  $Ca^{+2}$ ,  $Na^+$ ,  $K^+$ , and  $(SO_4)^+$  ions, the following concentration of chemicals recommended in [19] will be used in the pore solution:

- Saturated calcium hydroxide  $Ca(OH)_2$  (approx. 1.7 g/L)
- Sodium hydroxide  $Na(OH)$  (4.00 g/l)
- Potassium hydroxide ( $KOH$ ) (11.22 g/l)
- Calcium sulfate dehydrate  $Ca(SO_4) + 2H_2O$  (13.77 g/l)

The rebars will be placed in the pore solution as received without any special surface preparation in the area of study, since any form of special surface preparation affects the quality of the passive layer [3], [12], [41], and [47]. In addition, Ghods et al showed that no significant change in the anodic polarization of the rebar surface after being placed in the pore solution for 8 days or 14 days. Their results are shown in Fig. 3.4. Therefore the rebars will be placed in the pore solution for a minimum of 8 days.

To prepare the rebars for the development of the passive layer, a specimen preparation assembly will be developed. The assembly consists of placing the rebar inside a PVC pipe, closing the ends of the pipe with a 90° PVC elbow, and closing the open ends with PVC pipe plugs. The assembly is shown in Fig. 3.5. This assembly ensures that the pipe remains airtight and prevents the carbonation of the calcium hydroxide ( $Ca(OH)_2$ ) in the pore solution.

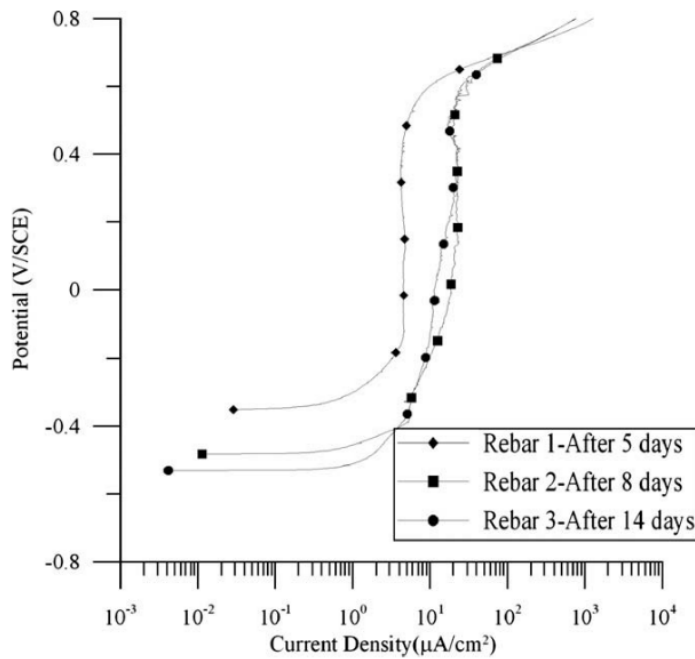


**Figure 3.4** As received rebars anodic polarization immersed in pore solution for different times[18]

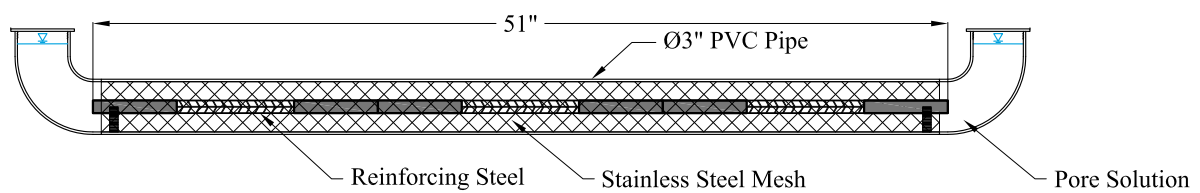


**Figure 3.5** Assembly for rebar preparation for the development of passive layer in pore solution

### Accelerated corrosion of reinforcing steel

Four components are required for corrosion to occur: (1) the anode, (2) the cathode, (3) an electrolytic connection, and (4) an electrical path. The corrosion cell that will be deployed in this study uses this concept in the following way: the anode consists of the rebar, the cathode consists of a stainless steel mesh, the electrolytic connection will be made with a sodium chloride solution, and the electrical path is forced via an electric circuit. The corrosion cell uses the assembly developed to generate the passive layer with the components needed for corrosion as shown in Fig. 3.6. The circuit was designed so that the current in the specimen is  $5mA$ , equivalent to  $47\mu A/cm^2$  on the bare surface of the rebar. Since the rebar and stainless steel mesh have a low resistance, a  $1k\Omega$  resistor will be added to the circuit, such that it stabilizes the current and keeps it constant at  $5mA$ .

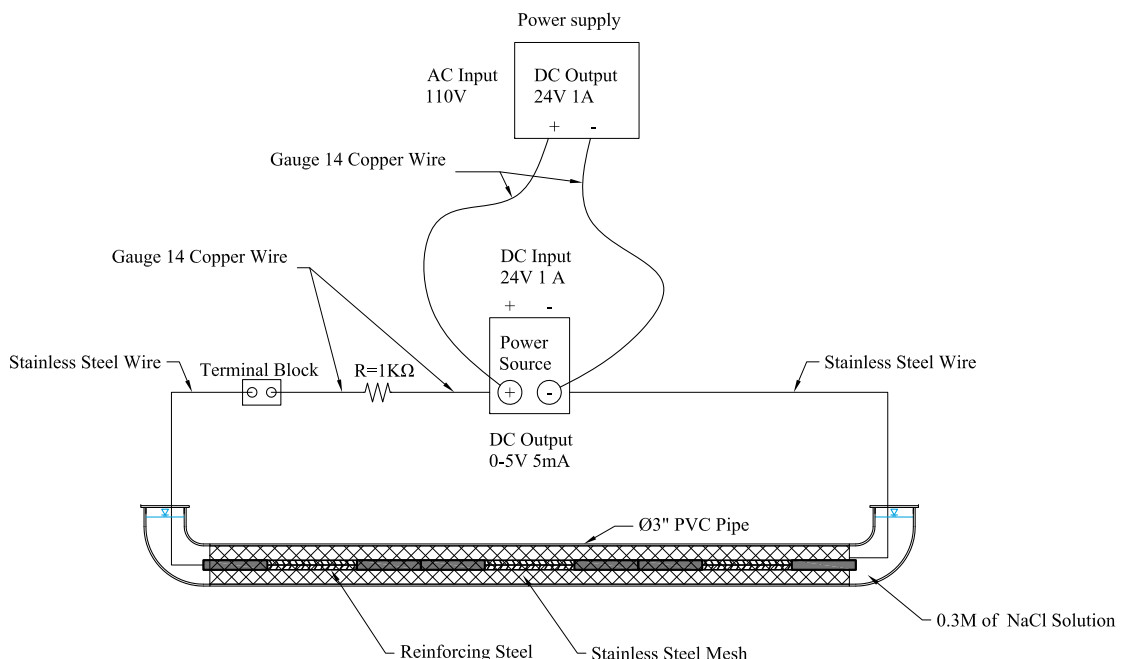


**Figure 3.6** Accelerated corrosion process

Ghods et al [19] determined that for rebars with passive films, a concentration of 0.3 Moles of sodium chloride ( $NaCl$ ) will start the depassivation process on the rebars. Accordingly ithe same sodium chloride solution will be used in this study. To estimate the time to apply the

current and obtain the desired level of corrosion, Faraday's law shown in equation 3.1 is used.

$$m_{loss} = \frac{it(AM)}{nF} \quad (3.1)$$

In equation 3.1,  $m_{loss}$  corresponds to the mass loss,  $i$  is the current in amperes ( $i = 5mA$ ),  $t$  is the time the current is sustained in seconds ( $AM$ ) is the atomic mass of the oxidizing component. For this study the oxidizing component is the iron ( $Fe$ ) in the rebars, hence  $(AM) = 54.845g/mol$ ,  $n$  is the number of electrons lost per atom oxidized, for  $Fe$  the number of electrons is equal to 2, and  $F$  is Faraday's number ( $F = 96485C$ ). Solving Eq. 3.1 for  $t$  and assuming uniform corrosion for different corrosion levels, the time of application is calculated. The estimated times to achieve the corrosion levels is shown in Table 3.1.

**Table 3.1** Accelerated corrosion times in 3/4" rebar

Corrosion Level (CL)	Mass loss (g)	time (days)
5%	0.93	7.5
10%	1.86	15
15%	2.80	22.5
20%	3.73	30
25%	5	37.3

### Tension tests

The tension tests will be performed to evaluate differences in the stress-strain behavior of corroded reinforcing steel with those found in the literature. In addition, the data obtained from these tests will serve as an input to the analytical model. Therefore, a series of tension tests will be performed accordingly. The tension tests will be performed in accordance with the standard ASTM A370, which specifies the loading procedure and the gauge lengths. The tension tests consist of:

1. Place the rebar in the universal testing machine
2. Pull the rebar in tension
3. Record the load and the strain on the rebar

The strains will be captured through the use of LED markers from the Optotrack Certus HD system. The gauge length between the LED markers will be 2inches as is specified in the

ASTM A370 standard, Fig. 3.7 shows an example of the test setup. The stress will be calculated based on the load reading from the UTM machine and divided by the measured area of the corroded rebars.



**Figure 3.7** Tension test setup example[44]

The results obtained from the tension tests will be valuable to understand the change in the stress-strain relationship, the yield strength, and ultimate strength of corroded rebars. Statistical analysis of the results will help to update equations that correlate these parameters to the corrosion level, and potentially yield an updated form of Eq. 2.6. The outcomes of the tension tests will further improve the results of the analytical model in Chapter 5.

### Buckled bar tension (BBT) test

One of the limit states considered in the seismic design of bridge columns is the buckling of rebar. Recent tests have been developed to determine the critical bending strain of buckled reinforcing steel [6], which is associated with the sudden fragile fracture of longitudinal reinforcement of RC column. The buckled bar tension (BBT) test simulates the bending and tension strain demands on a buckled bar to determine critical bending strain in buckled rebars.

Barcley et al [6] developed a methodology to calculate local strains on a buckled bar using an LED optical sensor system [43]. Fig. 3.8 shows the basic concept of the BBT test.

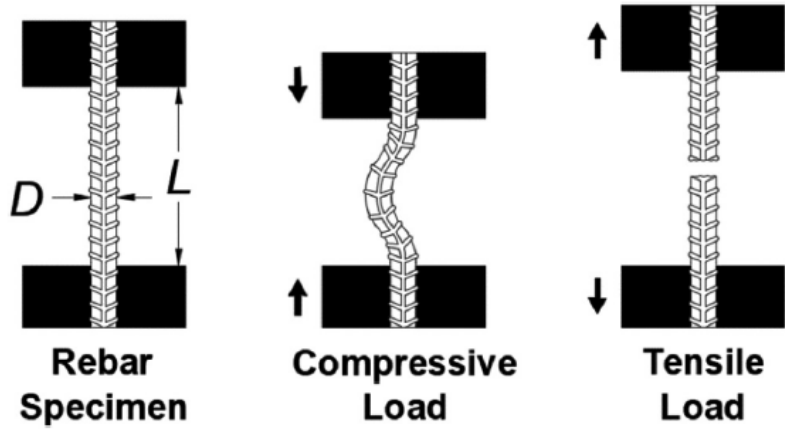


**Figure 3.8** BBT Test sequence[6]

The procedure to perform the buckled bar tension test consists of:

1. First, place rebar in a universal testing machine (UTM), and prepare the rebar specimen with LED markers on the surface of the specimen such that the displaced shape of the bar can be measured.
2. Second, compress the rebar specimen to impose a bending strain of a prescribed level. Barcley et al showed that a fourth order polynomial can be fit to the LED sensors near the buckled region of the bar to obtain the displaced shape ( $w$ ). The bending strain is calculated using solid mechanics principles. Curvature is the second derivative of the displaced shape ( $w$ ) for small displacements, which is calculated as:

$$\phi = \frac{\frac{d^2w(x)}{dx^2}}{\left[1 + \left(\frac{dw(x)}{dx}\right)\right]^{\frac{3}{2}}} \approx \frac{d^2w(x)}{dx^2} \quad (3.2)$$

If we assume that the bending is symmetric for the rebar then the strain in the extreme fibers of the rebar is calculated as:

$$\varepsilon_b = \phi \left( \frac{d_{bl}}{2} \right) \quad (3.3)$$

Combining equations Eq. 3.2, and Eq. 3.3, the bending strain can be expressed as:

$$\varepsilon_b = \frac{d^2w(x)}{dx^2} \left( \frac{d_{bl}}{2} \right) \quad (3.4)$$

An example of the calculation of the bending strain is shown in Fig. 3.9

3. Third, once buckled to the prescribed curvature, the bar is loaded in tension until fracture is observed
4. Then the process is repeated with a different bar for a different bending strain. After all the tests are performed results from elongation at peak force can be generated as the example shown in Fig. 3.11. From the results obtained through BBT tests the critical bending strain can be determined. The critical bending strain is defined as the point at which a low elongation under load is obtained. This low elongation results in a brittle fracture of the rebar as shown in Fig. 3.10(b). Fig. 3.11 shows that for bars with rebars the critical bending strain is  $\varepsilon_b = 0.10$  for grade 80 ksi steel.

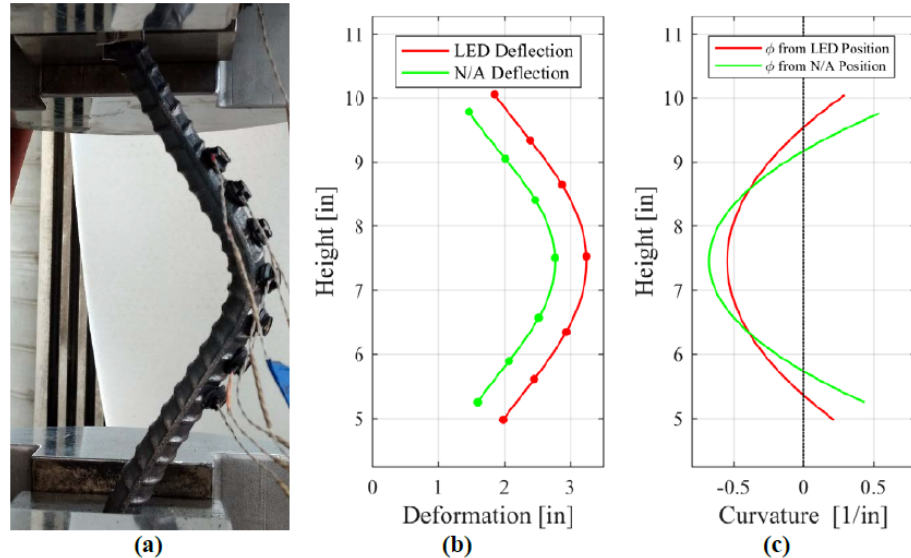


**Figure 3.9** a) Picture of buckled bar; (b) Position of optical markers and adjustment to neutral axis;  
(c) Calculation of curvature [5]



**Figure 3.10** (a)Ductile rebar fracture; (b) Brittle rebar fracture [5]

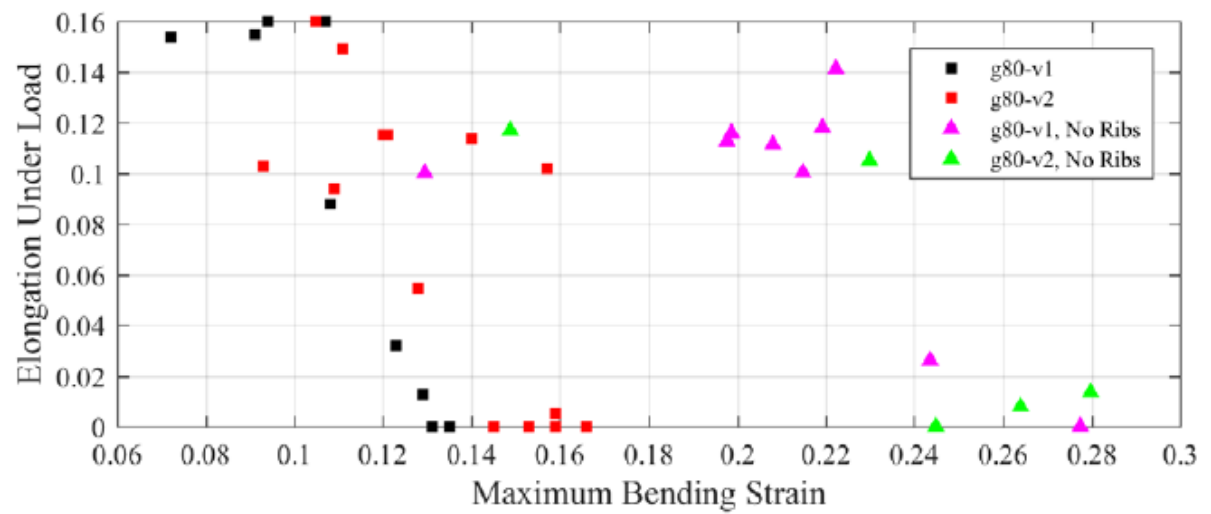


**Figure 3.11** BBT results for rebars with and without ribs [5]

The BBT tests are proposed for different levels of corrosion such that any changes on the behavior are studied and incorporated in the analytical model. The proposed test matrix is shown in Table 3.2. It must be noted that in each corrosion level for the BBT tests, each experiment will correspond to a different prescribed bending strain. The selection for each prescribed bending strains consist of 1) Start with the maximum bending strain determined in previous research to be around  $\varepsilon = 0.10$  as shown in Fig. 3.11, 2) if brittle fracture is observed the next test will be at a lower bending strain for example  $\varepsilon = 0.08$ , 3) otherwise higher strains such as  $\varepsilon = 0.12$  will be evaluated. This is repeated for each corrosion level. It is expected that six tests per corrosion level will be sufficient however, more tests will be performed if necessary. The results obtained will be compared to those of a pristine condition rebar which corresponds to a corrosion level of  $CL = 0\%$

**Table 3.2** Corroded Rebar Test Matrix

Corroded rebar test matrix			
Test	Diameter of bar	CL (%)	Number of Tests
Tension test	#6	0	3
		5	3
		10	3
		15	3
		20	3
		25	3
BBT test	#6	0	6
		5	6
		10	6
		15	6
		20	6
		25	6

### 3.2 Expected outcomes from experimental phase

The results from the tension tests will help to establish if the depassivation process in the corroded rebars has an effect on the measured stress-strain relationship of steel as has been observed in previous research that did not consider the depassivation process [37],[66],[13]. Similarly the results from the BBT tests will show any changes in the critical bending strain of rebars as they corrode. The critical bending strain impacts the bar fracture limit state. In the case of corroded rebars it is expected that the critical bending strain will be modified by changes in the mechanical properties of steel due to corrosion, and effects of concentrated corrosion will be visible along the surface of the rebars. We hypothesize that these two factors will induce fracture at a lower bending strain than those observed in pristine conditions rebars[6].

The results obtained from the experiment will also be used to define the bar fracture limit state for RC columns. Research currently being developed at NC State will provide models that allow us to establish bar fracture tensile strain while considering different parameters such as transverse steel spacing, axial load ratio, and strength of the concrete to mention a few. The model will be similar to that presented by Barcley et al [5] shown in Eq. 3.5.

$$\varepsilon_t = \frac{\ln(\frac{\varepsilon_b}{0.001})}{\frac{300p}{f'cA_g} + \frac{0.7}{\rho_t}} \quad (3.5)$$

This model could then be implemented in the analytical model presented in Chapter 5. If fracture occurs at a lower strain in corroded rebars, this implies that the corroded RC columns are prone to reach the fracture bar limit state at a much lower displacement than in a pristine RC column.

Future studies will verify the application of the results found in this research to perform full scale corroded RC column that consider the effect of depassivation in the cyclic behavior of such columns.

## Chapter 4

# Experimental Results from Corroded Rebar Specimens

The results from the experimental program are summarized in this chapter and the implications for structural design are evaluated.

### 4.1 Measurement of corrosion level

### 4.2 Tensions Tests

As described in Chapter 3, the bars were loaded in tension using the universal testing machine (UTM). The data collected corresponded to the Force using the UTM and the Optotrack system was used to calculate the strain.

During the tests it was observed that the failure usually occurred close to the grips. This is due to the sudden change in the cross section and the imperfections on the rebars. The strains used in this study correspond to the strain gauges located adjacent to the fracture. The fracture of these tests were brittle in nature, the appearance of necking was not significantly observable as shown in Fig. 4.1.

Fig. 4.2 show the stress-strain behavior for corrosion levels ranging from 0 - 20%. From this results, the yield strength, the uniform axial elongation, and the ultimate strength are obtained. From this results it appears that the effective yield strength and the effective ultimate strength reduce as the corrosion level increases. In addition, the stress strain curves results confirm that no necking significant necking was present, since were the after reaching the ultimate stress the bars suddenly drop in strength.

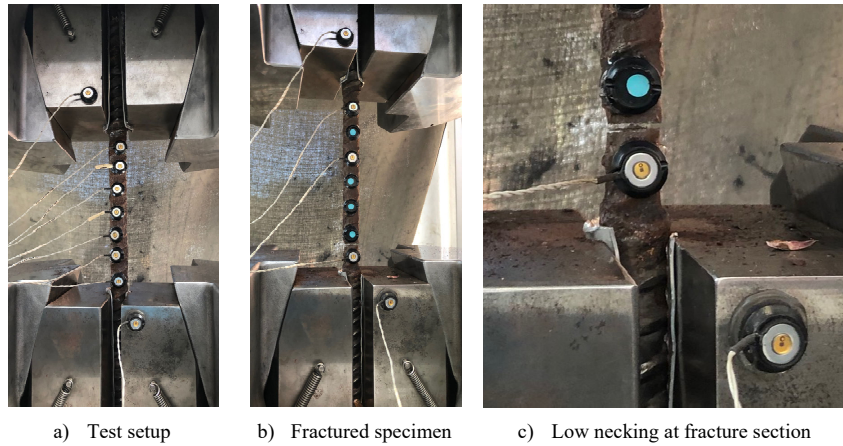


**Figure 4.1** Tension test setup and fracture observations

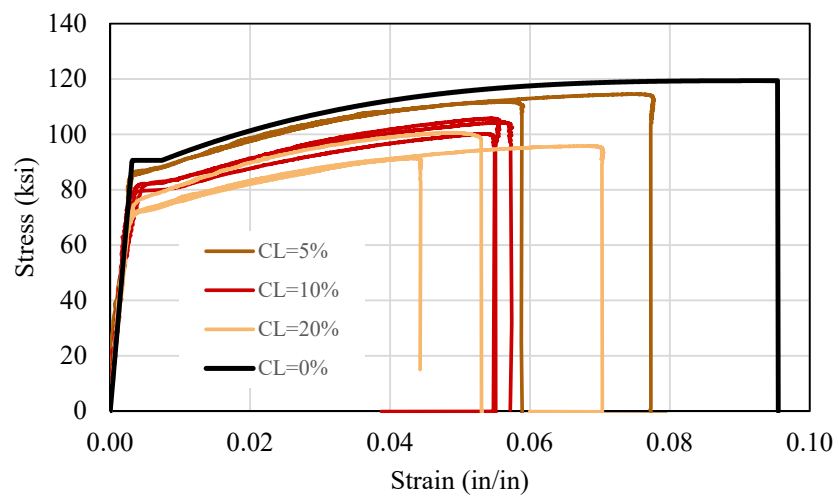


**Figure 4.2** Tension test results at different corrosion levels

#### 4.2.1 Yield strength as a function of corrosion

Fig. 4.3 shows the plot of the effective yield strength versus the corrosion level. The results show that there appears to be a linear relationship between them. This is congruent with other studies performed in other types of steel such as the study done by Du et al [13]. It has been studied that the apparent reduction in effective yield strength is due to points of concentrated reduction in the geometry of the rebars. Other studies [13][5] and this study, show that if the imperfections due to the corrosion are removed, then the properties of the virgin metal remain unchanged. What is observed in tension tests conducted on corroded rebars is an effective property that considers the imperfections in the geometry of the rebar.

The linear trend observed between the effective yield strength and the corrosion level can be expressed as:

$$f_{y,CL} = f_{y,o}(1 - 0.0075CL) \quad (4.1)$$

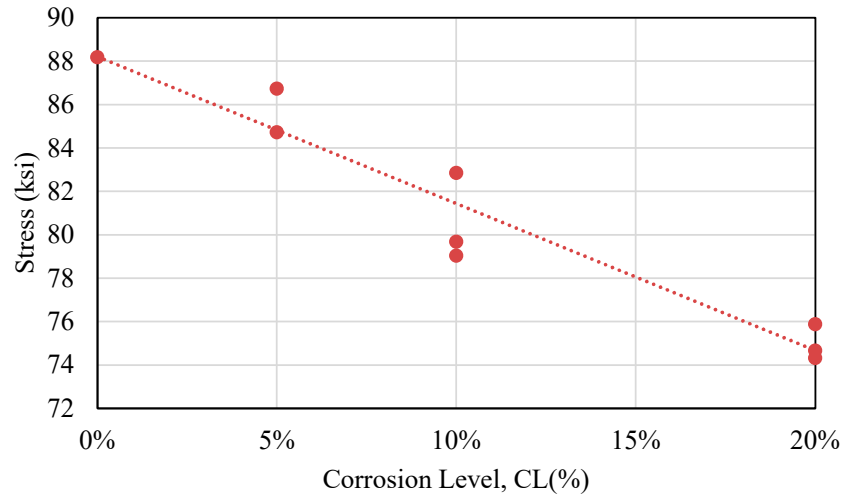


**Figure 4.3** Yield strength as a function of corrosion level

The proposed equation is compared to the one proposed by Du et al [13], replicated here as ???. From Fig. 4.4 we can observe that the existing model tends to over-predict the effective yield strength for Grade 80 steel. Therefore it is possible that there is correlation between corrosion level and the grade of the rebar, however the literature on corrosion for different grades of rebar is scarce.

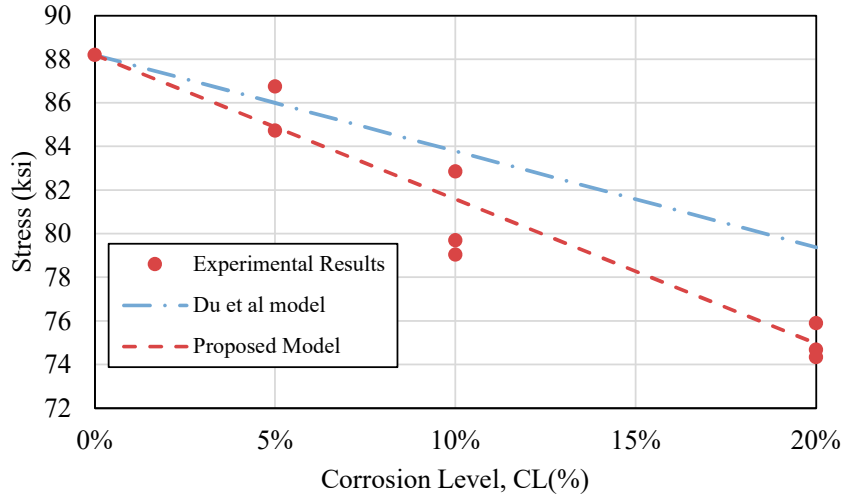


**Figure 4.4** Yield strength as a function of corrosion level comparison of proposed model and Du et al model [13]

#### 4.2.2 Effect of corrosion in uniform elongation

Another interesting result was observed on the uniform axial elongation property of the corroded rebars. As the rebar corrodes and develops more imperfections on the geometry of the rebar, it appears that the uniform axial elongation decreases. Fig. 4.5 shows this trend more clearly. However, after 10% corrosion the uniform axial elongation remains constant. This results may point towards why as structure corrode the level of perceived ductility is reduced and thus triggers an earlier failure than that observed on pristine structures.

We propose the following model to predict the uniform axial elongation of corroded grade 80 rebars:

For corrosion level between 0% - 10%

$$\varepsilon_{CL} = \varepsilon_o - 0.05CL \quad (4.2)$$

For corrosion level larger than 10%

$$\varepsilon_{CL} = 0.045 \quad (4.3)$$

While equations 4.1 - 4.3 are preliminary they provide an insight at the variations that different grades of rebar can have on the effective properties of corroded rebars.

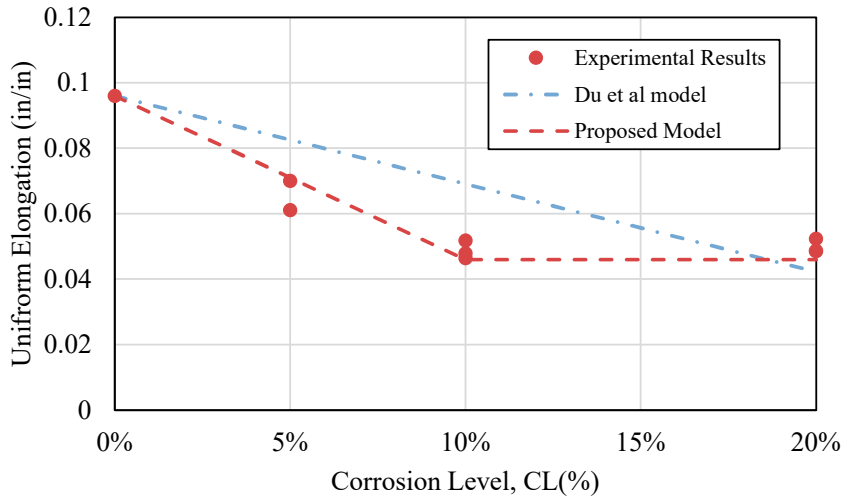


**Figure 4.5** Uniform elongation as a function of the corrosion level comparison of proposed model and Du et al model [13]

### 4.3 Buckled Bar Tension (BBT) Tests

#### 4.3.1 Summary of BBT procedure

The process of performing the buckled bar test consists of: 1) Loading the bar with the LED markers in the UTM machine. 2) Compress the bars to a prescribed level of bending strain. 3) Load the rebar in tension and 4) Record the type of fracture: Ductile or Brittle. This process is presented in Fig. 4.6.

The data obtained from the BBT test is then processed and two parameters are obtained: 1) the critical bending strain, based on the curvature, 2) the maximum uniform axial deformation is obtained from the stress strain curve. These two values are obtained as shown in Fig. 4.7. In the case of brittle failure if the bar does not elongate compared to its original length the uniform axial elongation is assigned a value of zero.

#### 4.3.2 Effect of corrosion in Critical Bending Strain

The buckled bar tension test was applied to rebars with varying levels of corrosion ranging from 0% - 20%. For each corrosion level a total of 6 BBT tests were performed, plotting the bending strain vs the uniform axial elongation, the critical bending strain is calculated as the point where the uniform axial elongation drops to zero. Fig. 4.8 summarizes the critical maximum bending

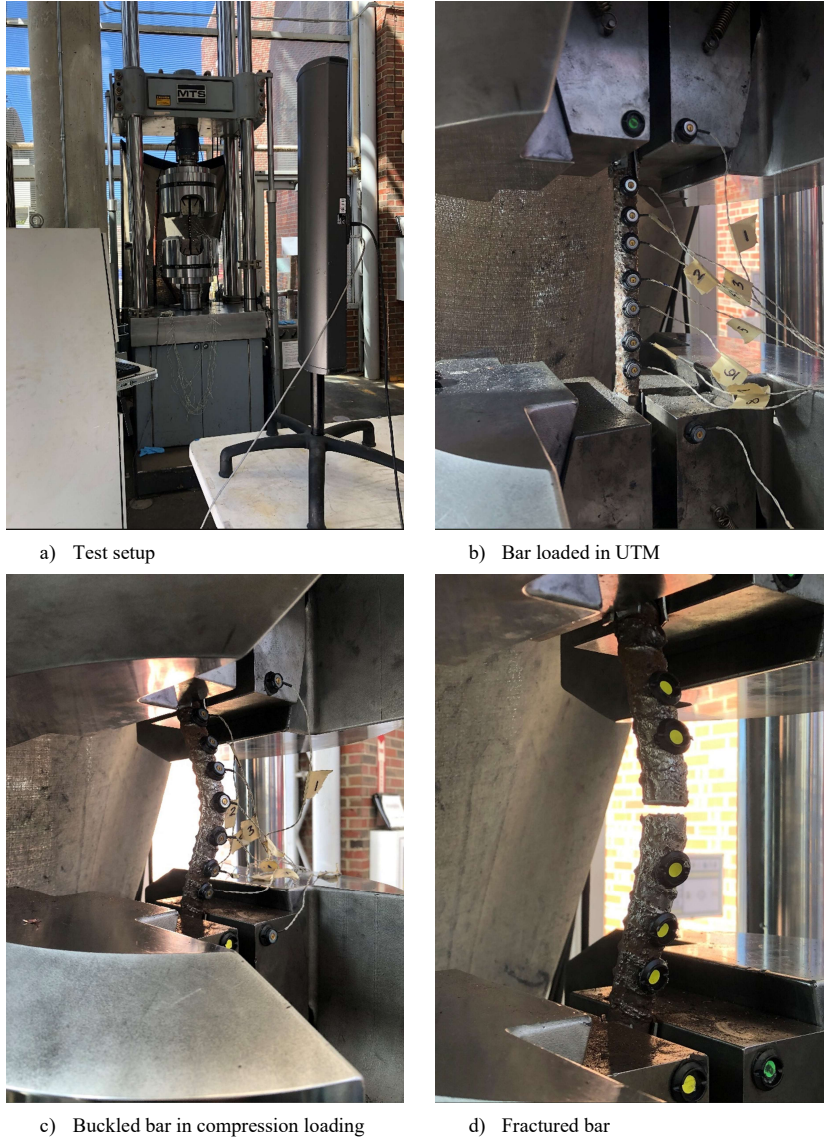


**Figure 4.6** General procedure of buckled bar tension (BBT) test

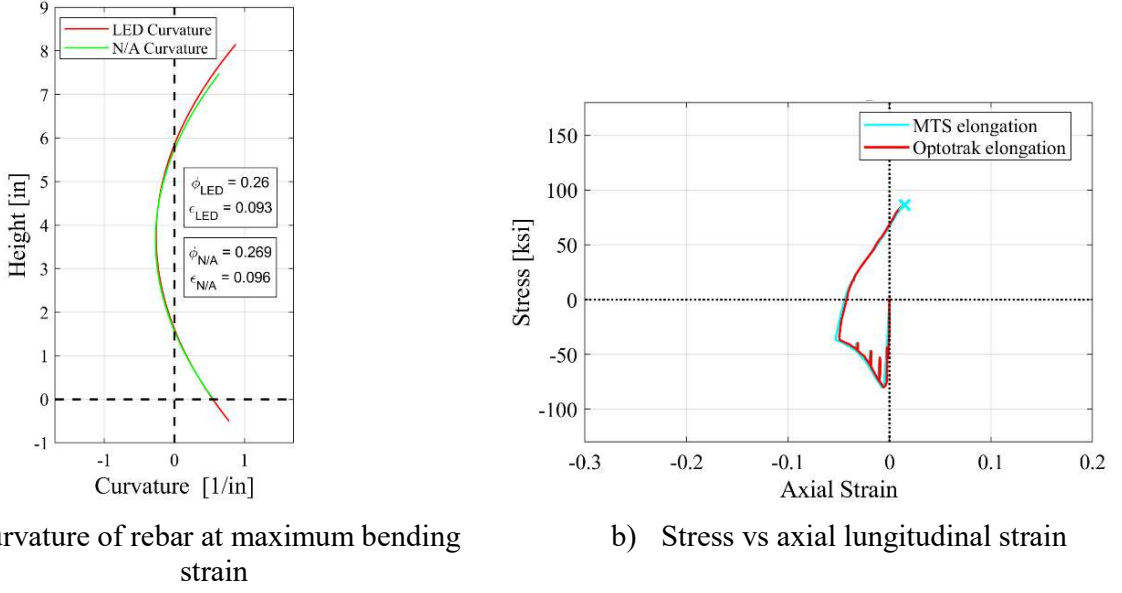


**Figure 4.7** Obtaining critical bending strain

strain at different corrosion levels including the benchmark value of pristine bars obtained by Barcley et al [5]. In Fig. 4.9 it is noticeable that as corrosion level increases the maximum bending strain reduces.

Fig. 4.9 shows the relationship between the critical bending strain and the corrosion level of the rebars. There is a linear relationship between both variables similar to the one observed in the tension tests. The relationship between corrosion level and critical bending strain ( $\varepsilon_b$ ) using linear regression can be expressed as shown below in 4.4.

$$\varepsilon_b(CL) = \varepsilon_o - 0.0045CL \quad (4.4)$$

It is interesting to notice the sharp drop in critical bending strain capacity as corrosion increases. For CL=5% There is a drop of about 20%, for CL=10% the change is 60% of the pristine condition and for CL=20% that difference is more than 140% decrease in the critical bending strain. This results indicate that there is a reduction in the ultimate capacity of rebars as they corrode. Based on this results and previous tests performed in corroded RC beams reported by Du et al [13], on RC columns as shown by Ma et al [31] and Meda et al [37], a limiting value for level of corrosion is CL=10%.

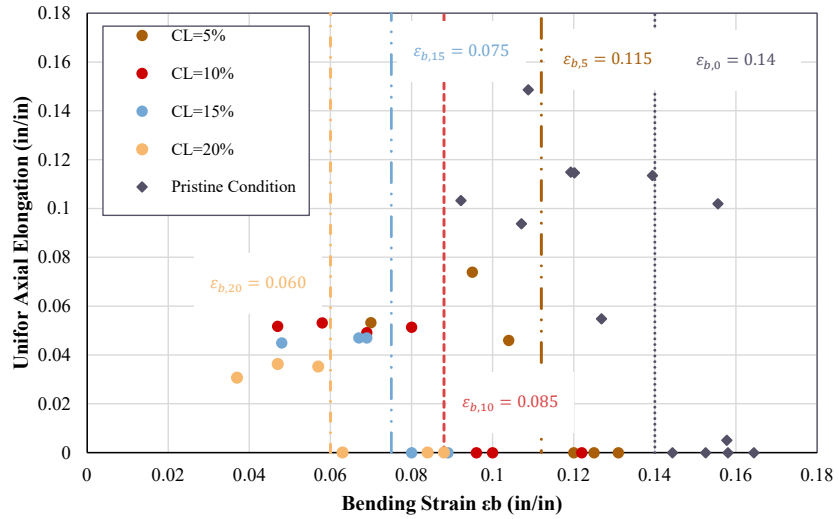


**Figure 4.8** Bending strain at different corrosion levels

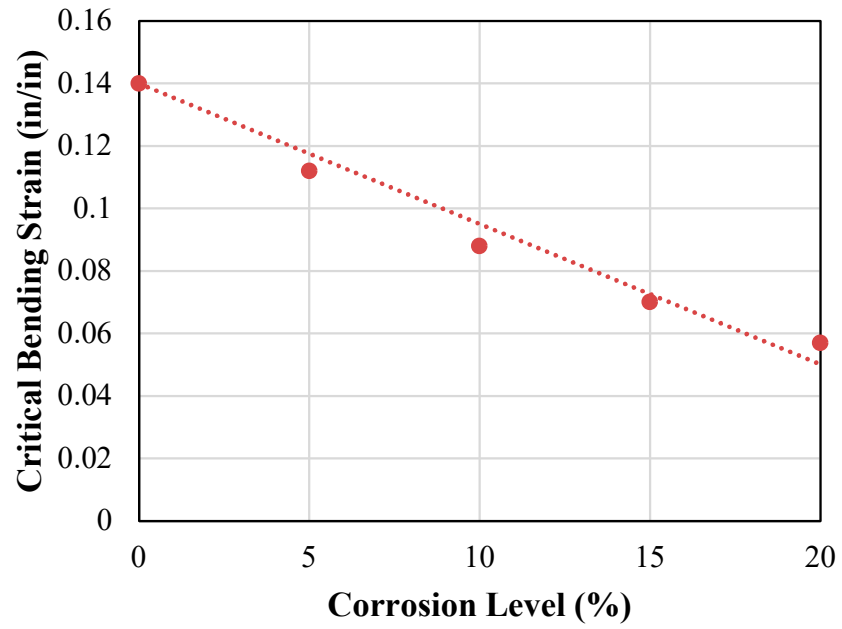


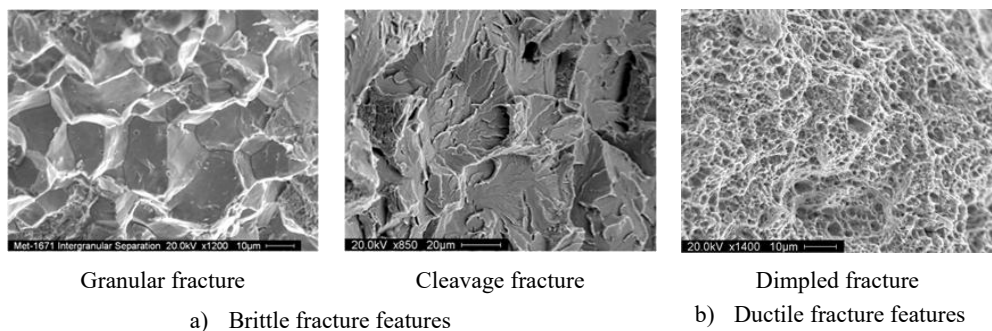
**Figure 4.9** Maximum bending strain as a function of corrosion level

#### 4.3.3 Effect of corrosion at the micro-structural level

To study if there was any change in the microstructural behavior of the rebars as they corroded and explore if the chlorides induced fracture in the rebars at the point of fracture, the rebar's fracture surfaces were observed under a variable pressure scanning electron microscope (VPSEM). Fracture surfaces from ductile and brittle failures were obtained at ductility levels of 5%-20%.

##### Fractography of BBT test specimens fracture surfaces

As previously observed in figure X, at the macro level brittle fractures typically consist of flat fracture surface, and in ductile fractures, there is necking and rougher edges along the fracture surface. The observations at the macro level translate into similar observations at the microstructural level. To analyze the images obtained from the Scanning Electron Microscope (SEM), it is important to understand how brittle and ductile fractures in metals look like in the SEM. Fig. 4.10 summarizes the typical features for brittle fractures and ductile fractures. Brittle fractures, present features that tend to promote flat surfaces, that two main types are granular and cleavage fractures. Ductile fractures on the other hand have dimple features, which due to the extension of the fracture surface at the point where atomic bonds are broken.



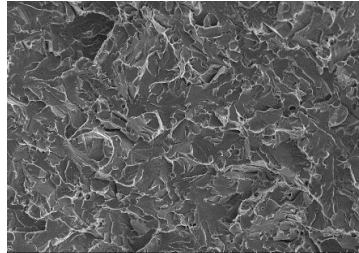
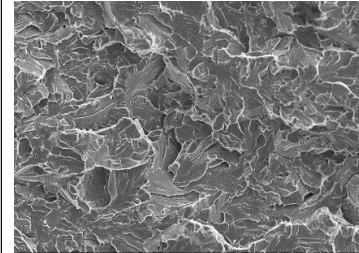
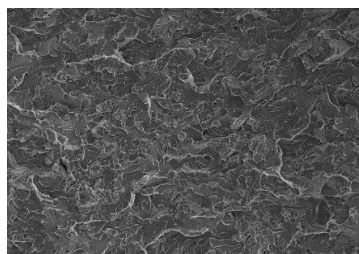
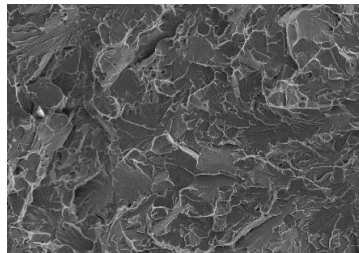
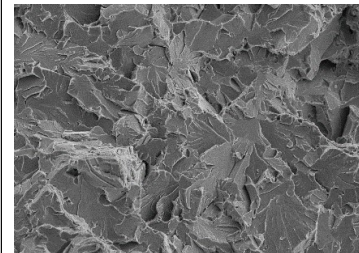
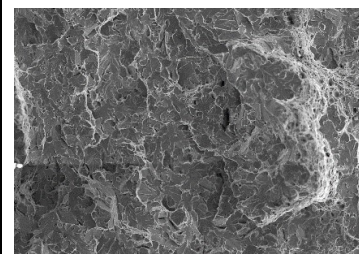
**Figure 4.10** Basic features analysis of fracture surfaces in metals

Fig. 4.11 summarizes the observations performed on the fracture surfaces. While VPSEM images were obtained for each corrosion level no substantial differences for brittle and ductile samples was observed as the corrosion level increased. Therefore, the observations performed on the CL=10% samples are shown here as representative of all the observations. The methodology of the observations was in such a way that differences between different sectors of the fracture provided comparison points. Fig. 4.11 shows three main sectors 1) point of initiation of fracture,

2) midpoint and 3) the extreme fiber opposite to the initiation of fracture. In all cases the point of initiation of fracture occurred where the extreme fiber was subjected to tension while being compressed.

Comparing the images obtained for the brittle and ductile response in Fig. 4.11 we can make the following observations. 1) At the point of initiation of fracture for the brittle and ductile surfaces there is no difference in the behavior of the fracture surfaces observed, indicating that the point of initiation of fracture is always brittle in nature, this can be seen in the presence of flat surfaces. 2) At the midpoint we can start to observe some differences for the brittle sample, flat surfaces are still observed but for the ductile sample, a mixture of flat surfaces and dimples typical of ductile surfaces are observed, this mixture of responses is similar to SEM observations of fracture surfaces of fatigue fractures. And 3) At the extreme fiber point the difference between ductile and brittle is more prominent since the ductile response has a predominant presence of dimples and the brittle response still shows flat surfaces. This results tell us the different mechanisms that occur between the brittle and ductile response and correlate well with the observed behavior of the BBT tests.

An important feature from the images obtained in the VPSEM observations was river like features observed through all the points of observations, as shown in Fig. 4.12. This type of features is typical of cyclic or fatigue tests, which is coherent with the BBT tests since the bar is loaded in compression and then loaded in tension.

Observation Location		Brittle failure	Ductile
Fracture Initiation	Center	Opposite extreme	Opposite extreme
			
			
			

**Figure 4.11** SEM observations for brittle and ductile failure at different positions of the fracture surface

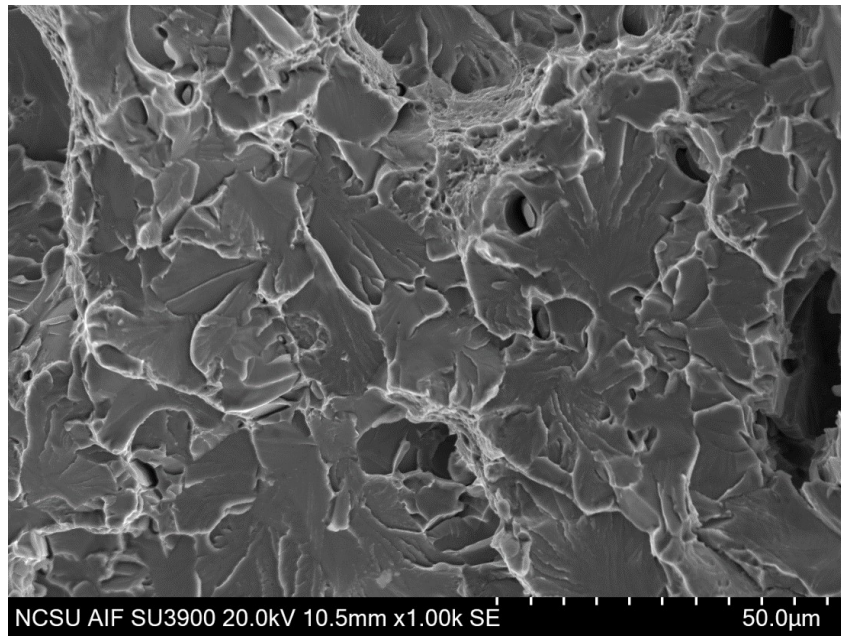


**Figure 4.12** SEM cyclic loading features in fracture surface at 500x magnification

### Spectrum analysis

In order to rule out the preclusion to failure due to inclusion of chlorides in the fracture surface a Back Scatter Electron (BSE) SEM images were evaluated through the use of spectrum analysis of the X-ray energy of the fracture surface. Fig. 4.13 shows the spectrum analysis of a brittle and ductile sample. The results obtained show elements that are expected on alloyed steel such as iron (Fe), carbon (C), chromium (Cr), Manganese (Mn), and vanadium (V), among others. But no presence of chlorides (NaCl) or oxides(O) was detected. Thus ruling out the onset of fracture due to the presence of these compounds.

#### 4.3.4 Effect of geometry imperfections

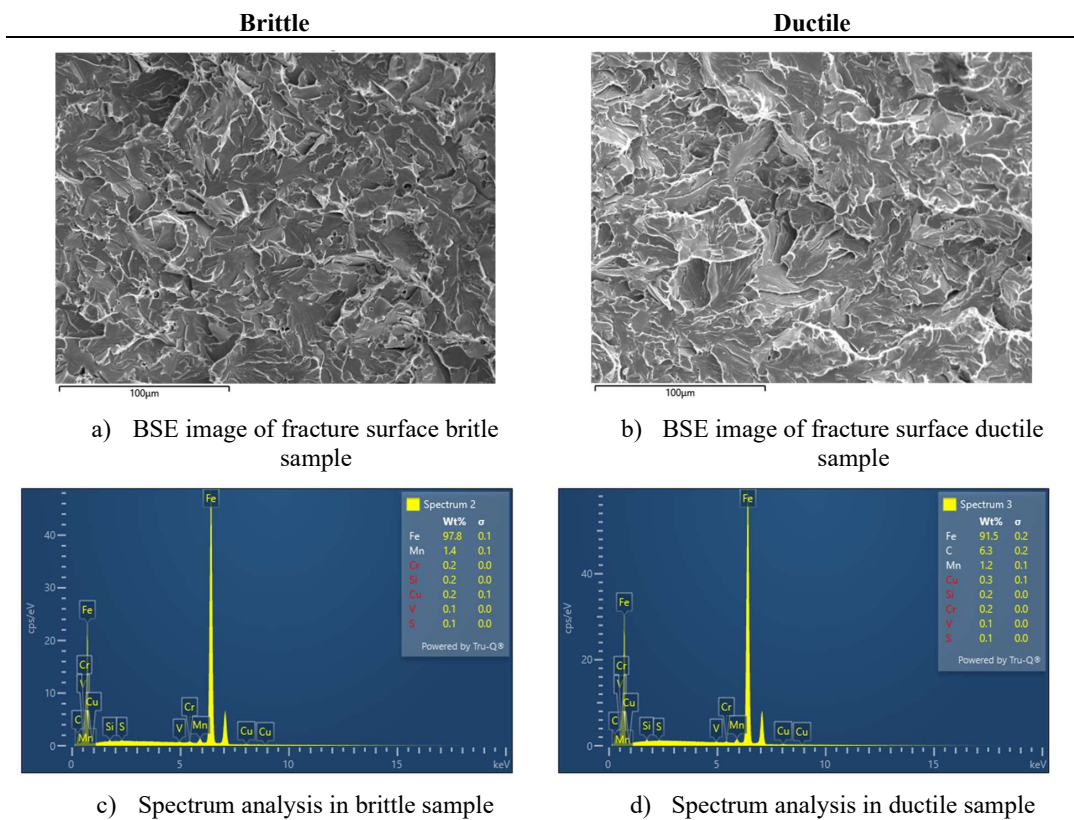


**Figure 4.13** Spectrum analysis of Back Scatter Electrons of fracture surface for brittle and ductile failures

# Chapter 5

## Analytical model

This research aims to develop a design procedure that incorporate the effect of cumulative damage in RC structures in order to improve their seismic resiliency. While previous studies have obtained results using the Ang and Park Damage Index and obtained fragility curves using the assumptions of that model, this research will evaluate the performance of structures using strain limit states. Therefore, an analytical model of a SDOF cantilever RC column will subjected to a series of nonlinear time history analyses (NLTHA) that consider aging conditions and sequences of mainshock and aftershock. The results of these analyses will record the limit state reached for each run of the analysis and we expect the results to show how the accumulation of damage due to aging of a structure increases the risk of a structure to reach a limit state.

### 5.1 Modeling of aging conditions

#### 5.1.1 Modeling of corrosion for structural analysis

It has been shown that as corrosion increases the material properties of the steel are modified, as discussed in section 2.1. While the findings from the material tests in Chapter 3 will show a more realistic quantification, we expect this trend to remain unchanged. The correlation between the level of corrosion and the mechanical properties of corroded rebars will be incorporated in the structural analysis. The workflow to modify the mechanical properties of the rebars is shown in Fig. 5.1. The modification of the mechanical properties consist of : (1) Calculate the time for initiation of corrosion with equation Eq. 2.2, (2) calculate the rate of corrosion with Eq. 2.3, (3) reduce the diameter of the rebar and calculate the corrosion level, using Eq. 2.5 and Eq. 2.4 correspondingly, and (4) modify the mechanical properties of the rebars with Eq. 2.6

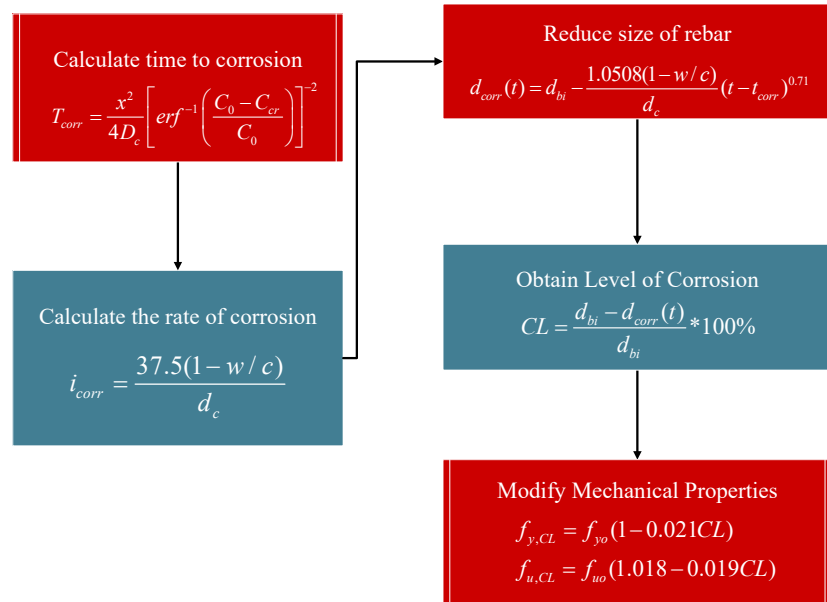


**Figure 5.1** Corrosion modeling for structural analysis

### 5.1.2 Modeling of strain aging for structural analysis

Strain aging modifies the properties of mild steel after being subjected to large strains, as explained in Chapter 2. Strain aging is of special relevance in the days following a mainshock. Consider the case of a structure, prone to strain aging, that is subjected to a mainshock and after more than 3 days is subjected to a large aftershock. This structure would behave differently during the aftershock due to the effects of strain aging. This situation is similar to that of the Canterbury Earthquake 2010 - Christchurch Earthquake 2011 sequence, since the ground motions struck in the same area of New Zealand, but occurred 5 months apart. To simulate this case scenario, the model proposed would consist of subjecting a series of SDOF structures to different mainshock-aftershock sequences. The main variable of study in this case would be the time between the mainshock and the aftershock, and the intensity measure of the ground motions. This procedure is explained in more detail in section 4.2.3.

## 5.2 Multiple seismic events

The evaluation of multiple seismic events is a topic that has been scarcely studied, however their effects have been felt in numerous earthquake sequences such as the Christchurch 2010,

Umbria-Marche Earthquake 1997 and the Puerto Rico Earthquakes 2020. The hypothesis is that accumulation of damage will restart in a smaller seismic event to achieve a prescribed limit state, similar to how corrosion and other aging phenomena might impact the intensity needed to achieve a future limit state.

For this study it has been determined that not all damage in structures are dependent on multiple events but rather their condition when an event occurs as is the case for corrosion. Therefore, in this study a Mainshock-Aftershock (MS-AS) sequence is evaluated at different levels of corrosion. Other damage related phenomena, such as strain aging, depend on the loading history and are therefore dependent on the history of extreme loading events. Thus, to study the effect on strain aging a sequences of mainshock-aftershock is focused on the time difference between the mainshock and the aftershock. The outcome will depend on the intensity of the ground motions and the pre-strain value achieved during the mainshock.

### 5.2.1 Earthquake selection

The earthquake selection will use two approaches to select the ground motions. The first consists of using the PEER web tool to perform amplitude scale matching of records that on average match the design spectrum. The second method involves conditional spectrum matching (CSM), which consists of computing the expected response spectrum associated with a target spectral acceleration ( $S_a$ ) value at a single period, using the information from the probabilistic seismic hazard analysis (PSHA).

In both selection methods it is necessary to define a design spectrum and the PSHA. Therefore, the city of Anchorage, AK is chosen to define the design spectrum and the PSHA. The design spectrum and the data are taken from the USGS PSHA webtool, which is shown in Fig. 5.2 and Fig. 5.3.

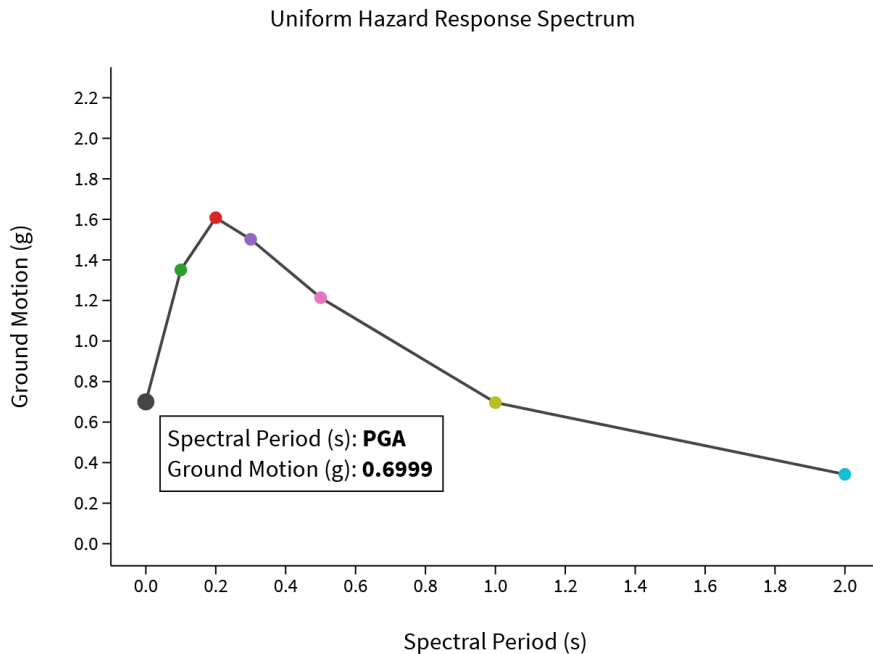


**Figure 5.2** Uniform Hazard Spectrum for Anchorage, AK

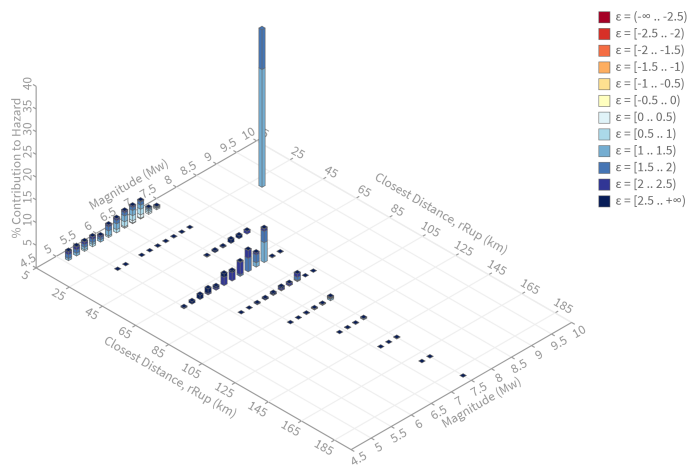


**Figure 5.3** PSHA deaggregation for Anchorage, AK

The ground motions are taken from the NGA2 West Database of earthquake records provided by the Pacific Earthquake and Engineering Research Institute (PEER) [2]. This database consists of 599 different earthquake events that characterize the ground motions on the west coast of the contiguous United States. The data was filtered according to the following criteria:

- Must be a mainshock-aftershock sequence
- Moment magnitude  $M_w \geq 5$
- $PGA > 0.04$
- $PGV > 1 \text{ cm/s}$
- $V_{s30} > 100 \text{ m/s}$  &  $V_{s30} < 1000 \text{ m/s}$
- Lowest usable frequency is less than 1Hz
- $R_{rup} < 60 \text{ km}$

Figure 5.4 summarizes the results from filtering the data available in the PEER NGA West2 database. Fig. 5.4 shows the earthquakes as moment magnitude Mw vs rupture distance ( $R_{rup}$ ).

### 5.2.2 Modeling of mainshock-aftershock series for corrosion damage state

Corrosion modifies the mechanical properties of rebars in RC structures, thus inherently modifying their response to earthquake loading. When an earthquake will occur is difficult to predict as explained in section 2.4.2. Therefore, in this study we propose subjecting structures at a specified corrosion level to a series of mainshock and aftershock ground motions. The proposed methodology will help to evaluate the effect of corrosion in RC structures subjected to earthquake loading with accumulation of damage. Specifically, the approach consists of (1) specify corrosion level (CL) as shown in Fig. 5.1, (2) the ground motions sequences from earthquake selection are applied for each corrosion level, (3) the results are evaluated in each case to determine what limit states were reached and the implication for the design proposal.

### 5.2.3 Modeling of mainshock-aftershock series for strain aging damage state

Strain aging consists of the increase in strength of steel after time has passed between a large strain and the new loading. It is possible that structures after being subjected to a mainshock develop the strain aging condition, especially if the maximum strain was higher than  $2\varepsilon_y$ . Therefore, the main variable of study for strain aging condition is the time between the main

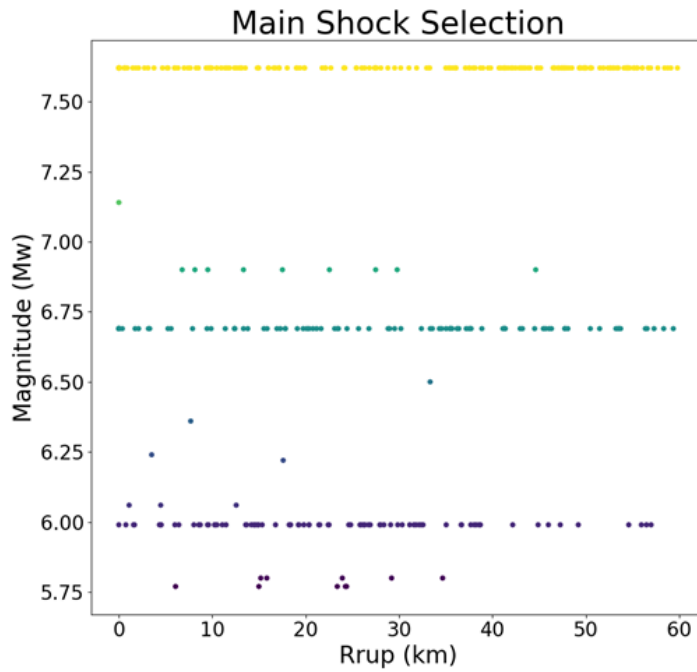


**Figure 5.4** Mainshock selection from PEER NGA West2 database

loading and the secondary loading. It is thus evident that the variable of study for strain aging is the time gap between the mainshock and the aftershock.

The proposed modeling of the mainshock-aftershock sequence in for strain aging consists of (1) the structure is subjected to the main shock, and the maximum strain in the rebar is recorded, (2) the time gap between the mainshock and the aftershock is varied between 3 days thorugh 50 days, (3) the mechanical properties of the rebar are modified according to Eq. 2.7 through Eq. 2.9, (4) the structure is evaluate for the aftershock groundmotion, and (5) the results are evaluated in each case to determine what limit states were reached and the implication for the design proposal.

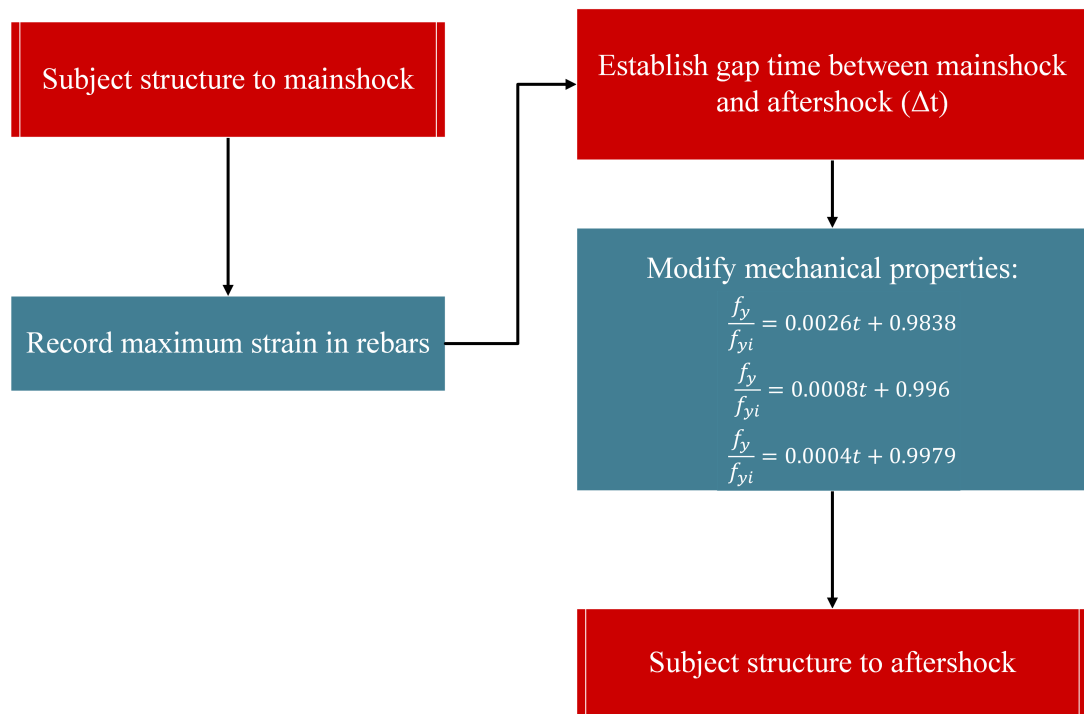


**Figure 5.5** Mainshock-aftershock modeling for strain aging

## 5.3 Analytical Model

### 5.3.1 Cantilever column

This study focuses on the behavior of a single degree of freedom (SDOF) system representing a cantilever reinforced concrete column. The column is modeled as shown in Fig. 5.6. This structure is modeled in OpenSeesPy [36][68] using the *forceBeamColumn* element [52]. The forceBeamColumn element is used with two-point Gauss-Radau integration applied in the hinge regions and two-point Gauss integration applied on the element interior for a total of six integration points [52]. The force-based formulation requires only a single element to accurately represent the full nonlinear deformation of the member and the integration scheme selected prevents the loss of objectivity during the softening response while also providing integration points at the member ends [9],[52]. The element requires the length of plasticity be defined at each end of the member, for which the tension-based rectangular plastic hinge length is calculated using the following expressions [23]:

$$L_{pc} = k * L_{eff} + 0.4D \quad (5.1)$$

$$k = 0.2 * (Fu/Fy - 1) \leq 0.08 \quad (5.2)$$

$$L_{pt} = L_{pc} + \gamma * D \quad (5.3)$$

For single bending the parameter  $\gamma$  is:

$$\gamma = 0.33 \quad (5.4)$$

The two-point Gauss-Radau integration is applied such that each end node integration is weighted equal to the specified plastic hinge length, as illustrated in Fig. 5.7. In this figure  $D$  is the diameter of the column, and  $c$  is the concrete cover. Therefore, strains recorded at the end sections represent accurate values even in the case where deformation localizes to the ends from strain-softening behavior. For the case of the cantilever column considered, only one plastic hinge length is defined, and the opposite end is given an arbitrary unit length.

The cross section of the column is shown in Fig. 5.8. The column cross section is discretized with concrete and steel material fibers. Concrete fibers are modeled using the *Concrete01* material, modified for confined material strength based on the Mander confined concrete model [35]. The *Steel02* material, based on the Giuffre-Menegotto-Pinto model [17] is used for the longitudinal reinforcement with recommended parameters ( $b = 0.01, R0 = 20, cR1 = 0.925, cR2 = 0.15$ ).

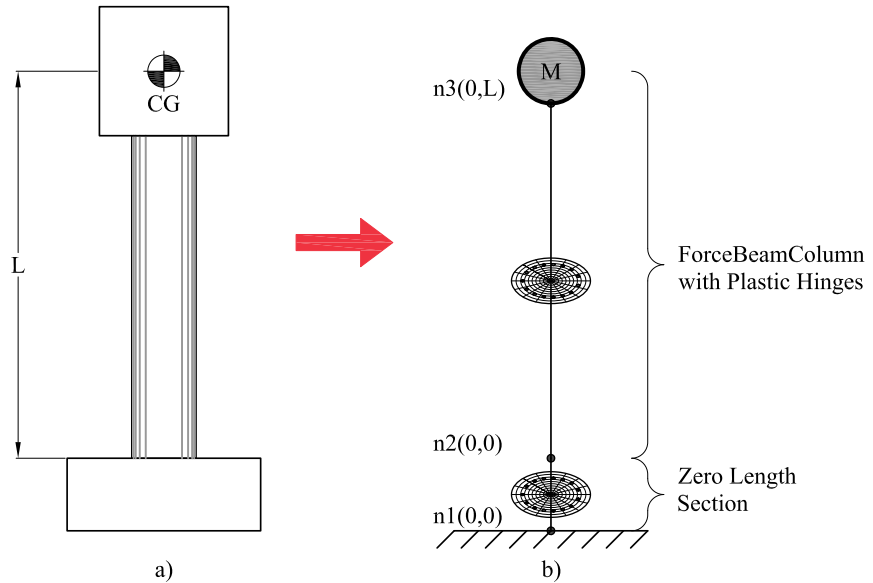


**Figure 5.6** Structural Model a) SDOF Column b) Structural Model

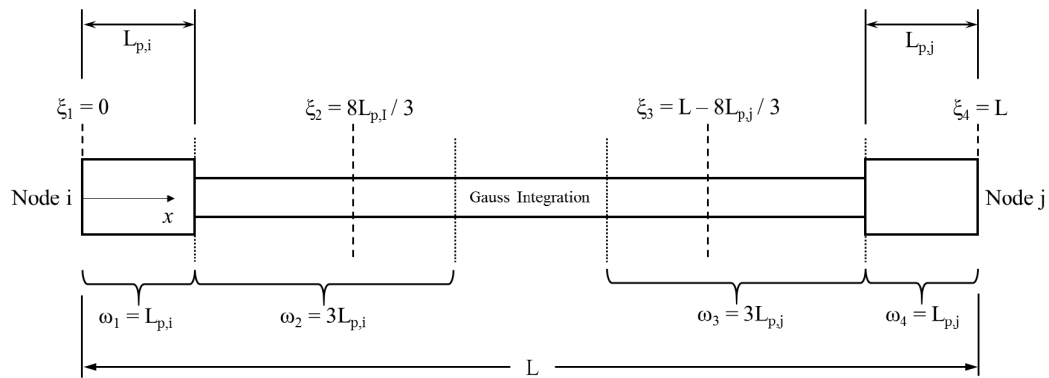


**Figure 5.7** End point plastic hinge method [52]

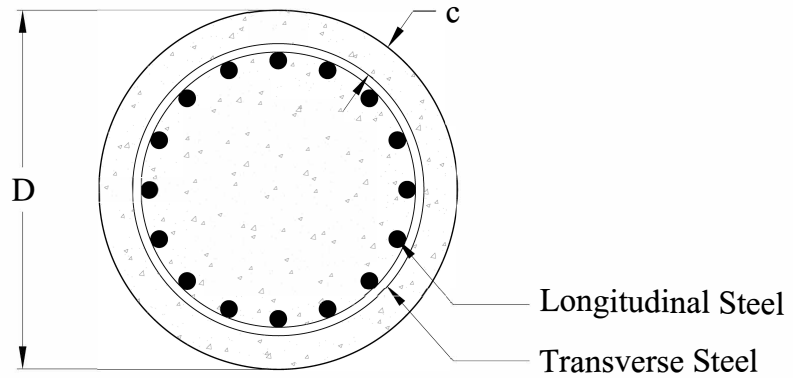


**Figure 5.8** Section of the RC Column

### 5.3.2 Strain penetration

The strain penetration considers the additional deformation due to anchorage of the reinforcement into the foundation, since tension strain in the reinforcement will drop to zero at a depth equal to the true development length of the rebar [48]. Experimental studies have generally reported that this end rotation contributes up to 35% to the lateral deformation of flexural members[67]. Therefore, it is important to incorporate it into the analytical model. A way to capture this effect is by using a zero-length section element implemented in the nonlinear fiber-based analysis of concrete structures, which is available in the material library of OpenSeesPy as *BondSP1* [67]. This is the material model used for the steel fibers of the zero-length section element.

The required parameters for this model are:

- $F_y$  Yield strength of the reinforcement steel
- $S_y$  Rebar slip at member interface under yield stress (see Eq. 5.5)
- $F_u$  Ultimate strength of the reinforcement steel
- $S_u$  Rebar slip at the loaded end at the bar fracture strength a value of  $35S_y$  is recommended [67]
- $b$  Initial hardening ratio in the monotonic slip vs. bar stress response  $b = 0.45$  is recommended [67]
- $R$  Pinching factor for the cyclic slip vs. bar response  $R = 1.01$  is recommended [67]

- $d_b$  Rebar diameter
- $f'c$  Concrete compressive strength of the adjoining connection member
- $\alpha$  Parameter used in the local bond-slip relation and can be taken as  $\alpha = 0.4$  in accordance with CEB-FIP Model Code 90 [11]

Bar slip is calculated as:

$$S_y(\text{in}) = 0.1 \left( \frac{d_b F_y}{4000 \sqrt{f'_c}} (2\alpha + 1) \right)^{\frac{1}{\alpha}} + 0.013(\text{in}) \quad (5.5)$$

### 5.3.3 Design limit states

Design limit states are defined based on strains in the material since they can more accurately represent the different performance levels of a structure. Structure limit states are defined as tension strains in the rebars or compression strains in the concrete core. The values recommended in typical performance-based design of reinforced concrete bridge columns are shown in Table 5.1. The serviceability limit states correspond to the compression strain at which concrete cover begins to crush and the peak tension strain which results in residual crack widths of approximately 1 mm. These limits are generally accepted as nominal limit states for RC members. The compression limit state for damage control is defined by the expression shown in Eq. 5.6, and it refers to the compression strain in the confined concrete at which fracture of the transverse reinforcement confining the core occurs [48]. This equation is obtained using the strain-energy balance between that absorbed by the confined core concrete and the capacity of the confining steel. The tension damage control limit state is defined by the strain at the onset of buckling which can be expressed according to 5.7. This model demonstrated accurate predictions of the onset of bar buckling on physical tests in SDOF Concrete Column [22]. The bar buckling limit state could change as a result of the experimental campaign proposed in Chapter 4.

$$\varepsilon_{c,spiralyield} = 0.009 - 0.3 \frac{A_{st}}{A_g} + 3.9 \frac{f_{yhe}}{E_s} \quad (5.6)$$

$$\varepsilon_{s,BB} = 0.03 + 700 \rho_s \frac{f_{yhe}}{E_s} - 0.1 \frac{P}{f'_c A_g} \quad (5.7)$$

**Table 5.1** Design limit states

Limit State	Concrete Limit State $\varepsilon_c$ (in/in)	Reinforcing Steel Limit State $\varepsilon_s$ (in/in)
Serviceability	0.004	0.015
Damage Control	Eq. 5.6	Eq. 5.7

## 5.4 Comparison with existing physical tests

The model used in this research is calibrated for the case of pristine conditions and the case of corroded columns. The calibration to a pristine condition column shows how reliable the results from the model are. Then the pristine condition model is modified with the corrosion model, as explained in section 4.1.1. The analytical model is compared to the results from the physical test on corroded RC columns. This will give confidence that the results obtained from the analytical model are reliable, and will be further enhanced with the experimental results.

### 5.4.1 Pristine condition columns

Goodnight et al performed a total of 30 circular RC columns quasi-static tests to evaluate strain limit states [22]. From this set of tests, a sample of one was taken to calibrate the analytical model. The test performed by Goodnight et al on an SDOF cantilever column shows similar geometry to that presented in Fig. 5.7. The parameters used in this large scale test were: diameter  $D = 24.0\text{inch}$ , height of the column  $L = 8.0\text{ft}$ , yield strength of steel  $f_y = 574.0\text{MPa}$ , ultimate strength of steel  $f_u = 753.3 * \text{MPa}$ , longitudinal steel volumetric ratio  $\rho_s = 1.5\%$ , transverse steel volumetric ratio  $\rho_v = 1.0\%$ , and strength of concrete at 8 days  $f'_c = 39.8\text{MPa}$ .

The analytical model used these parameters to compare the results from the model to the experimental results. The results from the analysis show good agreement with the experimental results as evidenced in Fig. 5.9. Thus, the results obtained from the model predict the overall system behavior and can be used to analyze other configurations of the structural model.

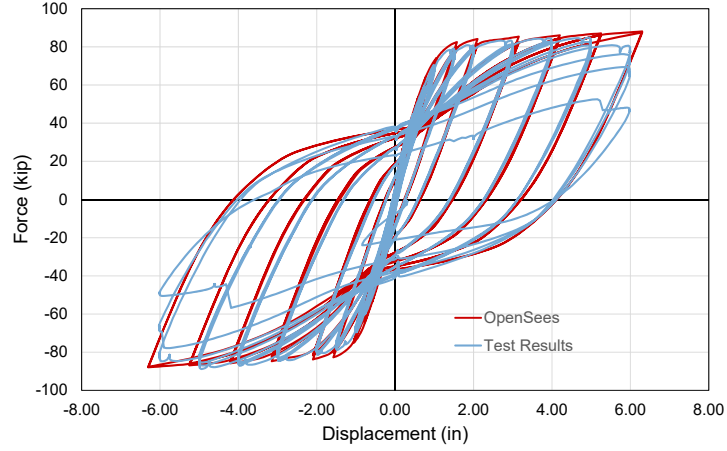


**Figure 5.9** Force-Displacement results from experimental results [23] and analytical model

#### 5.4.2 Accelerated corrosion columns

Similarly, Ma et al performed a series of quasi-static tests on RC columns with different corrosion levels and axial load ratios [31]. From their study, the test with a corrosion level  $CL = 9.5\%$  was taken for calibration since the other tests presented in their study had excessively high axial load ratios which are not common in RC bridges. The results from Ma et al test [31] were used to compare against the analytical model. The column had the following parameters: diameter  $D = 260.0\text{mm}$ , height of the column  $L = 820.0\text{mm}$ , yield strength of steel  $f_y = 375.0\text{ MPa}$ , ultimate strength of steel  $f_u = 572.3\text{ MPa}$ , longitudinal steel volumetric ratio  $\rho_s = 1.5\%$ , transverse steel volumetric ratio  $\rho_v = 1.0\%$ , strength of concrete at 8 days  $f'_c = 39.8\text{ MPa}$ , and corrosion level  $CL = 9.5\%$ . Equation 2.6 is used to modify the material properties of the reinforcing steel and considers the effects of corrosion.

Figure 5.10 shows that the results obtained from the analytical model capture the response of the structure with good accuracy. Ma et al [31] did not report if bar buckling and bar fracture occurred during the test. However, the hysteresis curve shown in their study suggests that some damage limit state was reached. Therefore, Eq. 5.7 is used to determine the bar buckling limit state ( $\varepsilon_{s,BB} = 0.024$ ), this is then compared to the analytical model results shown Fig. 5.11. The results show a peak tension strain of  $\varepsilon_s = 0.023$ , which is close to the value obtained using equation Eq. 5.7. Therefore, there is a high likelihood that the bar buckling limit state was reached during this test. While these results are close, it is still not clear if Eq. 5.7 captures the behavior of the buckling limit state for corroded rebars. Thus, the proposed corroded BBT test will show if corrosion affects the behavior of buckled bars.

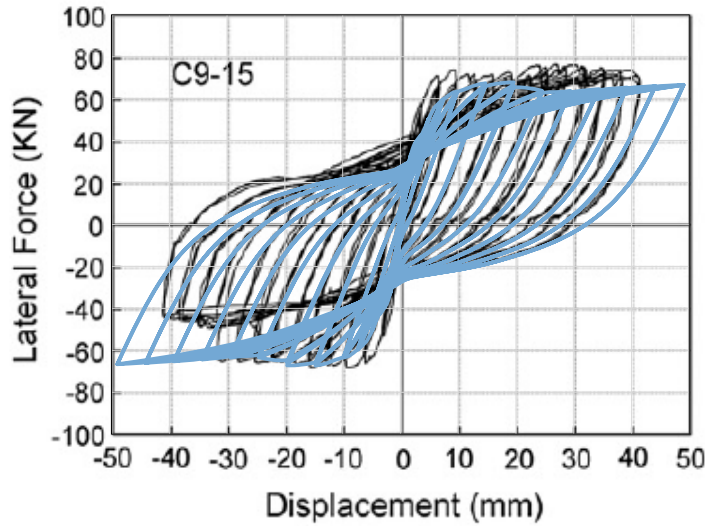


**Figure 5.10** Force-Displacement results from experimental RC column with corrosion in longitudinal bar (CL=9.5%) [31] and analytical model results (shown in lightblue)

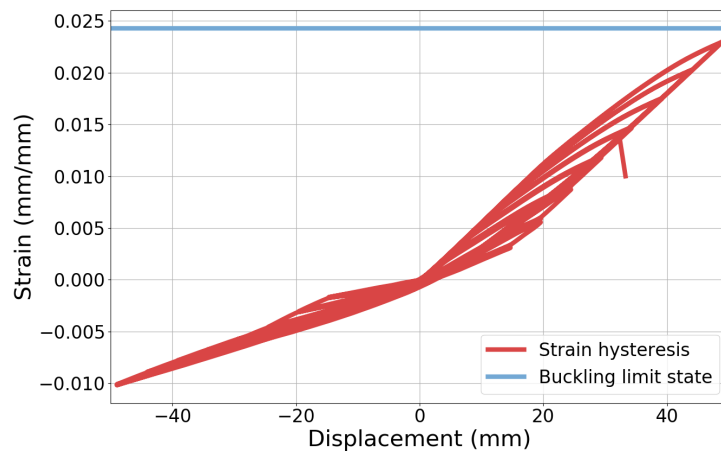


**Figure 5.11** Strain hysteresis from experimental RC column with corrosion in longitudinal bar (CL=9.5%) results from analytical model

## 5.5 Analytical framework

An analytical framework is established to obtain the change in the structure performance due to aging conditions and to evaluate the effect of multiple seismic events. Therefore, a series of nonlinear time history analyses (NLTHA) will be performed. From these analyses, it is possible to determine the effects of damage in the performance of structures. The proposed analytical framework process consists of:

1. Geometrical properties of the SDOF column
2. Properties of the material are evaluated (i.e. water to cement ratio, cover)
3. For equal periods of time the time dependent properties are modified
4. Nonlinear time history analyses are performed for discrete ground motions or sequence of ground motions
5. Results are obtained and evaluated

The analysis matrix for the corrosion aging phenomenon that will be analyzed in this study is shown in Table 5.2. The area or extent covered in the analysis corresponds to the range of variables that are common for RC columns in bridges.

**Table 5.2** Analysis matrix

ANALYSIS MATRIX		
Description	Parameter	Range
Diameter of column	D	30-90 in
Column length to diameter ratio	L/D	2-8
Longitudinal ratio	$\rho_s$	0.01-0.04
Transverse volumetric ratio	$\rho_v$	0.005-0.015
Axial load ratio	ALR	0.05-0.2
Water to cement ratio	w/c	0.36-0.6
Cover	c	1.5-3 in
Time/condition	CL	5%-20%

## 5.6 Results from NLTHA

This section presents the results obtained from a non-linear time history analysis (NLTHA) performed using OpenSeesPy [68]. The structure was subjected to a total of 18 earthquake records. The main responses obtained from these analyses correspond to the maximum strain obtained for the different levels of corrosion. The structure was analyzed for a range of corrosion levels [1.5%-13%] in the longitudinal rebars.

### 5.6.1 Effect on structure response

Figures 5.12 and Fig. 5.13 are presented as an example of the results obtained using NLTHA. These results are extracted from the response of the structure to the Chi-Chi earthquake. Fig. 5.12 shows the global system response and Fig. 5.13 shows the stress-strain response of the extreme fiber of reinforcing steel. These results show that as corrosion increases the demands imposed on the structure increases too. Therefore, the probability of reaching a limit state increases as corrosion increases.

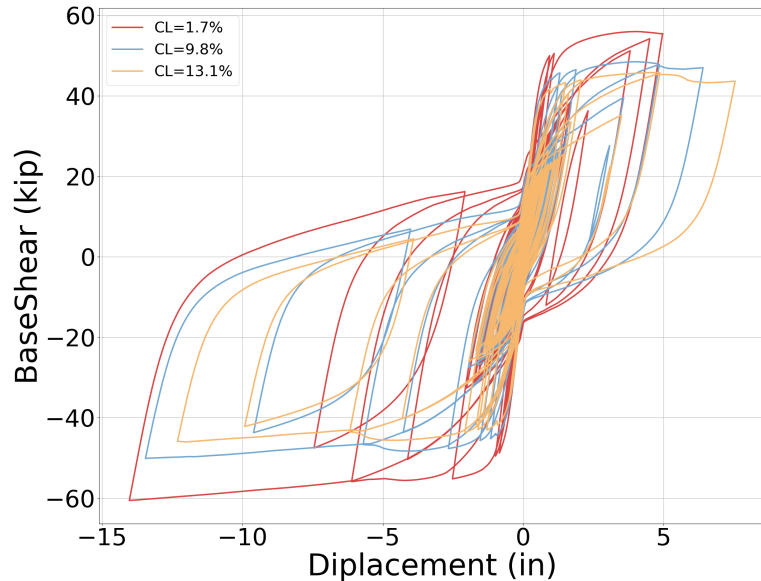


**Figure 5.12** Force-Displacement results

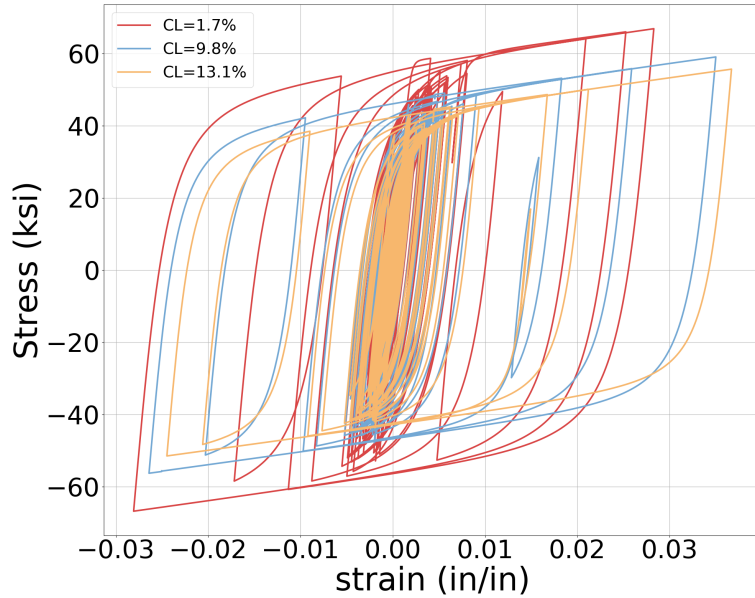


**Figure 5.13** Stress strain response for extreme rebar location

### 5.6.2 Development of cumulative distribution functions

Once the analysis is complete the data is post-processed and expressed as a cumulative distribution function (CDF). The methodology employed corresponds to the multiple stripe analysis (MSA) recommended by Baker et al [4]. While peak ground acceleration ( $PGA$ ) has been widely used as the intensity measure to develop fragility functions[21][7][54]. Krish [29] showed in a recent study, that spectral displacement at first effective period ( $IM = Sd(T_1)$ ) has better correlation than  $PGA$ . To demonstrate this, CDF curves were developed for  $IM = PGA$  and  $IM = Sd(T_1)$ , and are shown in Fig. 5.14 and Fig. 5.15 respectively. The CDFs were developed for the steel yielding limit state; however this can be extrapolated for any limit state. Fig. 5.14 shows the results obtained with  $IM = PGA$  do not show a good correlation since as corrosion increases the probability of exceeding a limit state decreases. This is not the behavior observed in Fig. 5.13. Conversely, Fig. 5.15 shows the results with  $IM = Sd(T_1)$ . These results present a better correlation, since, as corrosion increases, the probability of exceeding the limit state of yielding increases. For the preliminary results shown here, the corrosion level of 13.1% results are an exception. These results will improve as more analyses become available.

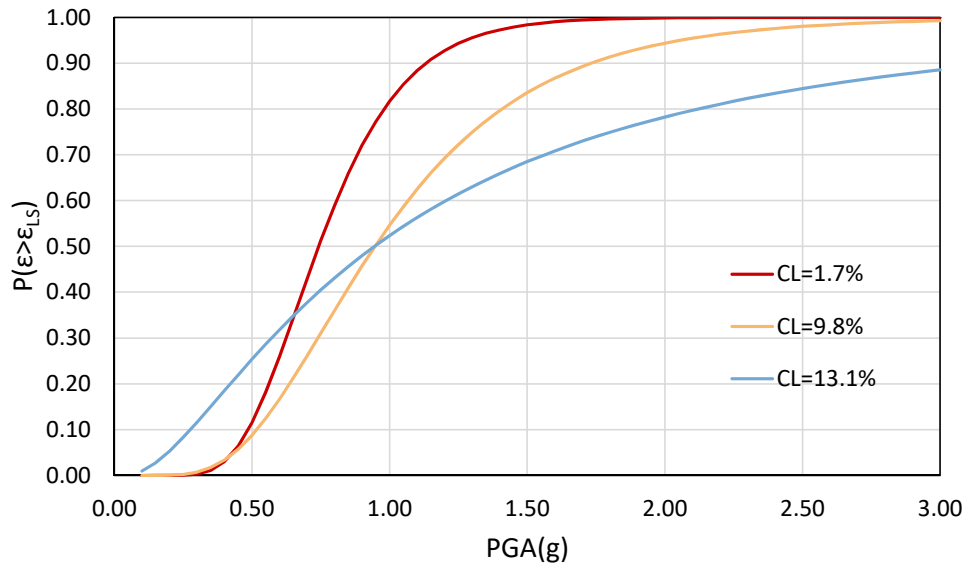


**Figure 5.14** CDF of steel yielding limit state using  $IM = PGA$

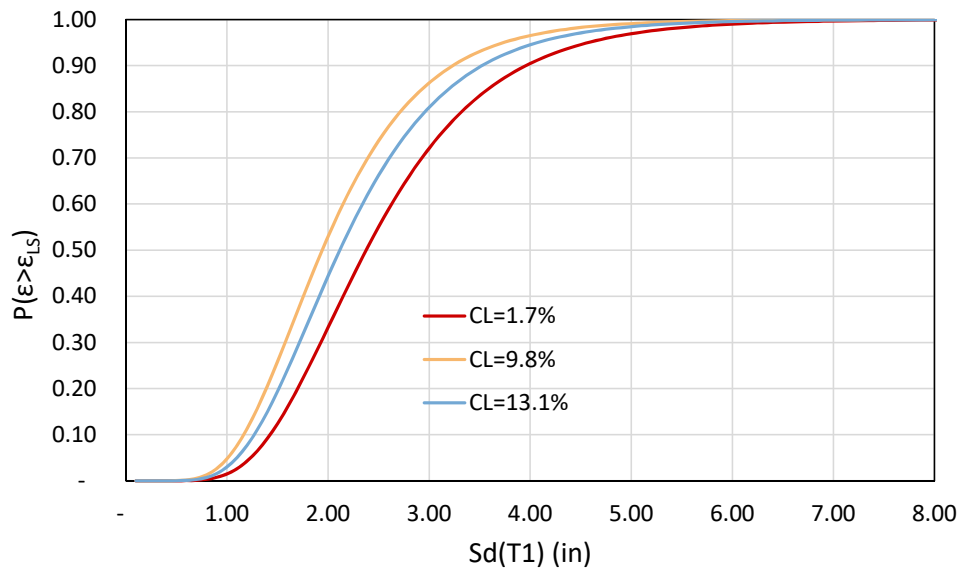


**Figure 5.15** CDF of steel yielding limit state using  $IM = Sd(T_1)$

### 5.6.3 Results discussion

The results show that there is an increase in the demands as the corrosion in the structure increases. This is clearly shown in Fig. 5.15. However, more results will help improve this correlation. In addition, the results shown in Fig. 5.14 and Fig. 5.15, demonstrate that  $IM = Sd(T_1)$  is a better intensity measure than  $IM = PGA$ .

Moreover, the outcomes from the experimental campaign will further improve the results obtained in the analytical work. The experimental phase will also provide an improved methodology to mimic the behavior of corroded reinforcing steel that is embedded inside the concrete, and the inclusion of additional aging conditions in the analysis will provide a realistic analysis of aging RC columns

## 5.7 Future topics

- Strength degradation in corroded RC structures
- Equivalent viscous damping in corroded RC structures
- Selection of intensity measure (IM)
- Degree of damage effect on confined structures behavior

## **Chapter 6**

# **Condition dependent performance based design and Assessment**

Developing a design procedure that provides resilient bridges is one of the main goals of this study. This research will develop a displacement based design tool, that achieves that goal. This chapter first introduces the overall design concept; then the direct displacement based design (DDBD) is reviewed and proposed modifications to this design methodology, based on corroded RC physical tests results, are shown. Finally a schedule of work is presented.

- 6.1 Recommendations to new designs from material tests**
- 6.2 Design of new structures with consideration of aging conditions**
  - 6.2.1 Existing methodologies**
  - 6.2.2 Proposed methodology**
  - 6.2.3 Application example: Bridge 547 (AKDOT)**
- 6.3 Assessment of existing structures considering aging conditions**
  - 6.3.1 Existing methodologies**  
ASCE 41 SLaMLA Priestley et al
  - 6.3.2 Proposed Condition Dependent Performance Based Seismic Assessment**
  - 6.3.3 Application Example: Bridge 547 (AKDOT)**

## **Chapter 7**

# **Conclusions and recommendations**

Developing a design procedure that provides resilient bridges is one of the main goals of this study. This research will develop a displacement based design tool, that achieves that goal. This chapter first introduces the overall design concept; then the direct displacement based design (DDBD) is reviewed and proposed modifications to this design methodology, based on corroded RC physical tests results, are shown. Finally a schedule of work is presented.

### **7.1 Conclusions**

### **7.2 Recommendations**

## BIBLIOGRAPHY

- [1] Amato, A., Azzara, R., Chiarabba, C., Cimini, G. B., Cocco, M., Di Bona, M., Margheriti, L., Mazza, S., Mele, F., Selvaggi, G., Basili, A., Boschi, E., Courboulex, F., Deschamps, A., Gaffet, S., Bittarelli, G., Chiaraluce, L., Piccinini, D. & Ripepe, M., "The 1997 Umbria-Marche, Italy, earthquake sequence: A first look at the main shocks and aftershocks," *Geophysical Research Letters*, **25**, no. 15, pp. 2861–2864, 1998.
- [2] Ancheta, T. D., Darragh, R. B., Stewart, J. P., Seyhan, E., Silva, W. J., S-J Chiou, B., Wooddell, K. E., Graves, R. W., Kottke, A. R., Boore, D. M., Kishida, T. & Donahue, J. L., "NGA-West2 Database," 2014.
- [3] Andersson, K., Allard, B., Bengtsson, M. & Magnusson, B., "Chemical composition of cement pore solutions," *Cement and Concrete Research*, **19**, no. 3, pp. 327–332, 1989.
- [4] Baker, J. W., "Efficient analytical fragility function fitting using dynamic structural analysis," *Earthquake Spectra*, **31**, no. 1, pp. 579–599, 2015.
- [5] Barcley, L., "Seismic Performance of A706-80 Reinforced Concrete Columns and Critical Bending Strain of Longitudinal Reinforcement," PhD thesis, North Carolina State University, 2018.
- [6] Barcley, L. & Kowalsky, M., "Critical Bending Strain of Reinforcing Steel and Buckled Bar Tension Test," *ACI Materials Journal*, **116**, no. 3, 2019.
- [7] Bisadi, V. & Padgett, J. E., "Explicit time-dependent multi-hazard cost analysis based on parameterized demand models for the optimum design of bridge structures," *Computer-Aided Civil and Infrastructure Engineering*, **30**, no. 7, pp. 541–554, 2015.
- [8] Bradley, B. A. & Cubrinovski, M., "NEAR-SOURCE STRONG GROUND MOTIONS OBSERVED IN THE 22 FEBRUARY 2011 CHRISTCHURCH EARTHQUAKE," Tech. Rep.
- [9] Calabrese, A., Almeida, J. P. & Pinho, R., "Numerical issues in distributed inelasticity modeling of rc frame elements for seismic analysis," *Journal of Earthquake Engineering*, **14**, no. sup1, pp. 38–68, 2010.
- [10] Choe, D.-E., Gardoni, P., Rosowsky, D. & Haukaas, T., "Probabilistic capacity models and seismic fragility estimates for RC columns subject to corrosion," *Reliability Engineering & System Safety*, **93**, no. 3, pp. 383–393, 2008.
- [11] Comité Euro-International du Betón, *CEB-FIP Model Code 90*, 1st. London, 1993.
- [12] Dawn Marcotte, T., "Characterization of Chloride-Induced Corrosion Products that form in Steel-Reinforced Cementitious Materials," PhD thesis, University of Waterloo, 2001.

- [13] Du, Y. G., Clark, L. A. & Chan, A. H. C., “Residual Capacity of Corroded Reinforcing Bars,” *Magazine of Concrete Research*, **57**, no. 3, pp. 135–147, 2005.
- [14] Enright, M. P. & Frangopol, D. M., “Probabilistic analysis of resistance degradation of reinforced concrete bridge beams under corrosion,” *Engineering Structures*, **20**, no. 11, pp. 960–971, 1998.
- [15] Fajfar, P., “Equivalent ductility factors, taking into account low-cycle fatigue,” *Earthquake Engineering & Structural Dynamics*, **21**, no. 10, pp. 837–848, 1992.
- [16] FEMA, “Prestandard and Commentary for the Seismic Rehabilitation of Buildings,” *Rehabilitation Requirements*, no. 1, pp. 1–518, 2000.
- [17] Filippou, F. C., Popov, E. & Bertero, V., “Effects of bond deterioration on hysteretic behavior of reinforce concrete coint,” Tech. Rep. August, 1983, p. 212.
- [18] Ghods, P., Isgor, O. B., McRae, G. & Miller, T., “The effect of concrete pore solution composition on the quality of passive oxide films on black steel reinforcement,” *Cement and Concrete Composites*, **31**, no. 1, pp. 2–11, 2009.
- [19] Ghods, P., Isgor, O. B., McRae, G. A. & Gu, G. P., “Electrochemical investigation of chloride-induced depassivation of black steel rebar under simulated service conditions,” *Corrosion Science*, **52**, no. 5, pp. 1649–1659, 2010.
- [20] Ghosh, J. & Padgett, J. E., “Aging Considerations in the Development of Time-Dependent Seismic Fragility Curves,” *Journal of Structural Engineering*, **136**, no. 12, pp. 1497–1511, 2010.
- [21] Ghosh, J., Padgett, J. E. & Sánchez-Silva, M., “Seismic Damage Accumulation in Highway Bridges in Earthquake-Prone Regions,” *Earthquake Spectra*, **31**, no. 1, pp. 115–135, 2015.
- [22] Goodnight, J. C., Kowalsky, M. J. & Nau, J., “Strain limit states for circular rc bridge columns,” *Earthquake Spectra*, **32**, no. 3, pp. 1627–1652, 2016.
- [23] Goodnight, J. C., Kowalsky, M. J. & Nau, J. M., “Effect of load history on performance limit states of circular bridge columns,” *Journal of Bridge Engineering*, **18**, no. 12, pp. 1383–1396, 2013.
- [24] Hatzigeorgiou, G. D. & Beskos, D. E., “Inelastic displacement ratios for SDOF structures subjected to repeated earthquakes,” *Engineering Structures*, **31**, pp. 2744–2755, 2009.
- [25] Hosseini, S., Heidarpour, A., Collins, F. & Hutchinson, C. R., “Effect of strain ageing on the mechanical properties of partially damaged structural mild steel,” *Construction and Building Materials*, **77**, pp. 83–93, 2015.

- [26] Jensen, O. M., Hansen, P. F., Coats, A. M. & Glasser, F. P., “Chloride ingress in cement paste and mortar,” *Cement and Concrete Research*, **29**, no. 9, pp. 1497–1504, 1999.
- [27] Khashaee, P. & Eeri, M, “Damage-based Seismic Design of Structures,” *Earthquake Spectra*, **21**, no. 2, pp. 371–387, 2005.
- [28] Krawinkler, H., “Performance Assessment of Steel Component,” *Earthquake Spectra*, **3**, no. 1, pp. 27–41, 1987.
- [29] Krish, Z. F., “Rapid Repair of Reinforced Concrete Bridge Columns Subjected to Seismic Loading via Plastic Hinge Relocation,” PhD thesis, North Carolina State University, 2018.
- [30] Kunnath, S. K., Reinhorn, A. M. & Lobo, R. F., “IDARC Version 3.0: A Program for the Inelastic Damage Analysis of RC Structures,” **818**, no. 1992, pp. 1–20, 1992.
- [31] Ma, Y., Che, Y. & Gong, J., “Behavior of corrosion damaged circular reinforced concrete columns under cyclic loading,” *Construction and Building Materials*, **29**, pp. 548–556, 2012.
- [32] Mackie, K. R. & Stojadinović, B., “Performance-based seismic bridge design for damage and loss limit states,” *Earthquake Engineering & Structural Dynamics*, **36**, no. 13, pp. 1953–1971, 2007.
- [33] Mackie, K. R. & Stojadinović, B., “Seismic demands for performance based design of bridges,” *Pacific Earthquake Engineering Research Center, PEER Repor*, no. August, p. 156, 2003.
- [34] Manafpour, A. R. & Kamrani Moghaddam, P., “Performance capacity of damaged RC SDOF systems under multiple far- and near-field earthquakes,” *Soil Dynamics and Earthquake Engineering*, **116**, pp. 164–173, 2019.
- [35] Mander, J. B., Priestley, M. J. N. & Park, R., “Theoretical stress-strain model for confined concrete,” *Journal of Structural Engineering*, **114**, no. 8, pp. 1804–1826, 1988.
- [36] McKenna, F., Scott, M. H. & Fenves, G. L., “Nonlinear finite-element analysis software architecture using object composition,” *Journal of Computing in Civil Engineering*, **24**, no. 1, pp. 95–107, 2010.
- [37] Meda, A., Mostosi, S., Rinaldi, Z. & Riva, P., “Experimental evaluation of the corrosion influence on the cyclic behaviour of RC columns,” *Engineering Structures*, **76**, pp. 112–123, 2014.
- [38] Mehta, P. K. & Monteiro, P. J. M., *Concrete: Microstructure, Properties, and Materials*, 4th ed. McGraw Hill, 2014.

- [39] Miranda, E., Archbold, J., Heresi, P., Messina, A., Rosa, I., Robertson, I., Mosalam, K., Kijewski-Correa, T., Prevatt, D. & Roueche, D., “PRJ-2712 — StEER - Puerto Rico Earthquake Sequence December 2019 to January 2020: Field Assessment Structural Team (FAST) Early Access Reconnaissance Report (EARR),” Structural Extreme Events Reconnaissance, Tech. Rep., 2020, p. 173.
- [40] Momtahan, A., Dhakal, R. P. & Rieder, A., “Effects of strain-ageing on New Zealand reinforcing steel bars,” *Bulletin of the New Zealand Society for Earthquake Engineering*, **42**, no. 3, pp. 179–186, 2009.
- [41] Moragues, A., Macias, A. & Andrade, C., “Equilibria of the chemical composition of the concrete pore solution. Part I: Comparative study of synthetic and extracted solutions,” *Cement and Concrete Research*, **17**, no. 2, pp. 173–182, 1987.
- [42] NIED K-NET KiK-net, *K-NET, KiK-net*, 2019.
- [43] Northern Digital Inc., *OPTOTRAK Certus HD dynamic measuring machine*, 2020.
- [44] Overby, D., “Stress-Strain Behavior of ASTM A706 Grade 80 Reinforcement,” PhD thesis, North Carolina State University, 2016.
- [45] Overby, D., Kowalsky, M. & Seracino, R., “Stress-strain response of A706 grade 80 reinforcing steel,” *Construction and Building Materials*, **145**, pp. 292–302, 2017.
- [46] Padgett, J. E. & Desroches, R., “Bridge Functionality Relationships for Improved Seismic Risk Assessment of Transportation Networks,” *Earthquake Spectra*, **23**, no. 1, pp. 115–130, 2007.
- [47] Page, C. L. & Vennesland, “Pore solution composition and chloride binding capacity of silica-fume cement pastes,” *Matériaux et Constructions*, **16**, no. 1, pp. 19–25, 1983.
- [48] Priestley, M., Calvi, G. M. & Kowalsky, M. J., *Displacement-Based Seismic Design of Structures*, 1st. Pavia, Italy: IUSS Press, 2007.
- [49] Raghunandan, M., Liel, A. B. & Luco, N., “Aftershock collapse vulnerability assessment of reinforced concrete frame structures,” *Earthquake Engineering & Structural Dynamics*, **44**, no. 3, pp. 419–439, 2015.
- [50] Restrepo-Posada, J., Dodd, L. L., Park, R & Cooke, N, “Variables Affecting Cyclic Behavior of Reinforcing Steel,” *Journal of Structural Engineering*, **120**, no. 11, pp. 3178–3196, 1994.
- [51] Roufaiel, M. S. L. & Meyer, C., “Analytical modeling of hysteretic behavior of r/c frames,” Tech. Rep.

- [52] Scott, M. H. & Fenves, G. L., “Plastic Hinge Integration Methods for Force-Based Beam-Column Elements,” *Journal of Structural Engineering*, **132**, no. 2, pp. 244–252, 2006.
- [53] Shearer, P. M., *Introduction to seismillogy*, 2nd editio. Cambridge: Cambridge University Press, 2009, pp. 301–320.
- [54] Shekhar, S., Ghosh, J. & Padgett, J. E., “Seismic life-cycle cost analysis of ageing highway bridges under chloride exposure conditions: modelling and recommendations,” *Structure and Infrastructure Engineering*, **14**, no. 7, pp. 941–966, 2018.
- [55] Stewart, M. G. & Rosowsky, D. V., “Time-dependent reliability of deteriorating reinforced concrete bridge decks,” *Structural Safety*, **20**, no. 1, pp. 91–109, 1998.
- [56] Sunasaka, Y. & Kiremidjian, A. S., “A method for structural safety evaluation under mainshock-aftershock earthquake sequences,” Stanford University, Tech. Rep., 1993.
- [57] Tesfamariam, S., Goda, K. & Mondal, G., “Seismic Vulnerability of Reinforced Concrete Frame with Unreinforced Masonry Infill Due to Main Shock-Aftershock Earthquake Sequences,” *Earthquake Spectra*, **31**, no. 3, pp. 1427–1449, 2015.
- [58] Thoft-Christensen, P., “Corrosion and Cracking of Reinforced Concrete,” *Life-Cycle Performance of Deteriorating Structures: Assessment, Design and Management*, 2003, pp. 26–36.
- [59] Vamvatsikos, D. & Allin Cornell, C., “Incremental dynamic analysis,” *Earthquake Engineering and Structural Dynamics*, **31**, no. 3, pp. 491–514, 2002.
- [60] Vu, K. A. T. & Stewart, M. G., “Structural reliability of concrete bridges including improved chloride-induced corrosion models,” *Structural Safety*, **22**, no. 4, pp. 313–333, 2000.
- [61] Weyers, R. E., Fitch, M. G., Larsen, E. P., A1-Qadi, I. L., Chamberlin Albany, W. P., York, N. & Hoffman, P. C., “Service Life Estimates,” Strategic Highway Research Program, Washington DC, Tech. Rep., 1994.
- [62] Williams, M. S. & Sexsmith, R. G., “Seismic Damage Indices for Concrete Structures: A State-of-the-Art Review,” *Earthquake Spectra*, **11**, no. 02, pp. 319–349, 1995.
- [63] Y. Liu & R. E. Weyers, “Modeling the Time to Corrosion Cracking in Chloride contaminated Reinforced Concrete Structures,” *ACI Materials Journal*, **95**, no. 6, pp. 675–680, 1998.
- [64] Yang, S.-Y., Song, X.-B., Jia, H.-X., Chen, X. & Liu, X.-L., “Experimental research on hysteretic behaviors of corroded reinforced concrete columns with different maximum

- amounts of corrosion of rebar,” *Construction and Building Materials*, **121**, pp. 319–327, 2016.
- [65] Young-Ji Park, B., H-S Ang, A. & Asce, F, “Mechanistic seismic damage model for reinforced concrete,” *Journal of Structural Engineering*, **111**, no. 4, pp. 722–739, 1985.
  - [66] Yuan, Z., Fang, C., Parsaeimaram, M. & Yang, S., “Cyclic Behavior of Corroded Reinforced Concrete Bridge Piers,” *Journal of Bridge Engineering*, **22**, no. 7, 2017.
  - [67] Zhao, J. & Sritharan, S., “Modeling of strain penetration effects in fiber-based analysis of reinforced concrete structures,” *ACI Structural Journal*, **104**, no. 2, pp. 133–141, 2007. arXiv: [arXiv:1011.1669v3](https://arxiv.org/abs/1011.1669v3).
  - [68] Zhu, M., McKenna, F. & Scott, M. H., “OpenSeesPy: Python library for the OpenSees finite element framework,” *SoftwareX*, **7**, pp. 6–11, 2018.